2017-10-14

LONGITUDINAL VARIATIONS OF PHASE SCINTILLATION DURING GEOMAGNETIC STORM

AGEGNEHU, SISAY

LONGITUDINAL VARIATIONS OF PHASE SCINTILLATION DURING GEOMAGNETIC STORM

SUBMITTED TO THE SCHOOL OF GRADUATE STUDIES OF BAHIR DAR UNIVERSITY IN PARTIAL FULFILLMENT OF THE REQUIREMENTS FOR THE DEGREE OF MASTER OF SCIENCE IN PHYSICS

By

AGEGNEHU SISAY

BAHIR DAR UNIVERSITY

BAHIR DAR, ETHIOPIA

JUNE 2017

BAHIR DAR UNIVERSITY

DEPARTMENT OF

PHYSICS

The undersigned here by certify that they have read and recommend to the college of Science, School of Graduate Studies for acceptance a project entitled "Longitudinal variations of phase scintillation during geomagnetic storm" by AGEGNEHU SISAY in partial fulfilment of the requirements for the degree of Master of Science.

Dated June 2017

Advisor: Tsegaye Kassa (PhD)

Internal examiner: _____

External examiner: _____

Examination Committee: _____

_____

_____

BAHIR DAR UNIVERSITY

Date: June 2017

Author: Agegnehu Sisay

Title: VARIATIONS OF PHASE SCINTILLATION DURING GEOMAGNETIC STORM

Department: Physics

Degree: M.Sc. Convocation: June Year: 2017

Permission is here with granted to Bahir Dar University to circulate and to have copied for non-commercial purposes, at its discretion, the above title upon the request of individuals or institutions

_____

Signature of Author

THIS PROJECT IS DEDICATED TO MY FATHER, ATO SISAY BIRHAN DERESE, MY MOTHER, W/O YALGA NIGATU BELAY, MY SPONSOR MR.BEYENE AND MY BRATHERS AND SISTERS.

Table of content

List of figure

List of Abbreviation

GNNS ------Global Navigations Satellite System

GPS --------Global Position System

TEC --------Total Electron Content

ROT --------Rate of Total Electron Content

ROTI ------ -Rate of Total Electron Content Index

IPP ----------Ionospheric Pierce Point

EEJ ---------Equatorial Electro Jet

SED --------Storm Enhancement Density

HF ----------High Frequency

VHF ------- Very High Frequency

SAPS ------- Sub Aurora Polarization Stream

DST --------Disturbance Storm Time

IPB ---------Ionospheric Plasma Bubble

STEC ----- -Slant Total Electron Content

VTEC ------ Vertical Total Electron Content

PRN --------Pseudo Random Noise

IMF -------- Interplanetary Magnetic Field

UT ---------- Universal Time

CME -------Coronal Mass Ejection

CIR ---------Co-rotating Interaction

SSC---------Sudden Storm Commitment

H ----------Horizontal Magnetic Field

Bz ---------- Magnetic Field Along Z-direction

GRT --------Gravitational Rayleigh Taylor

Es ----------Equatorial Sporadic -E

MHz --------Mega Hertz

UV ---------Ultra Violate

EUV -------Extreme Ultra Violate

List of table

Acknowledgements

First and foremost I would like to thank the Almighty God for all the things he has done for me. I am very much indebted to thank respectfully my Advisor **Dr.** Tsegaye Kassa, for his scientific guidance which helped me to identify the research problem and accomplish this thesis research work in particular and to work hard in all aspects of life in general. It is a pleasure to convey my gratitude to people whose contribution is great to my work. In the first place I would like to record my gratitude to Dr Melssew Nigussie for his supervision, advice, and guidance from the very early stage of this research as well as giving me extraordinary experiences throughout the work. I would also acknowledge Habtamu Marew and Fasil Tesema for their constructive help. My special thank go to my family whose support is not expressible with words. I greatly acknowledge my sponsor Mr. Beyene to help me by financial, motivation and morals.

Abstract

In this study we analysed the longitudinal variations of phase scintillation during geomagnetic storm by using VTEC,ROT &ROTI on March 16-18, June 22-23 and December 19-21/ 2015.We used GPS data of TEC for selected days with IGS stations codes and geomagnetic coordinates from North America in Canada: CAGS(45.6°N, 75.8°W) & ESCU(47.1°N,64.79°W) and world Europe in Italy:BGRZ-(46.49°N,11.3°E),Ukraine: MIKL(47.0°N,32.0°E),Switzerland:ZIMM(46.9°N,7.5°E),Slovakia:GANP(49.0°E,20.3°E)and Austria: GANP(47.1°N,15.5°E). The geomagnetic storm data was taken from Kyoto University. The Material was used to studied this study using UNAVCO down load software, GGrun 2016 ,and matlab The TEC data are downloaded from UNAVCO data home page http://facility.unavco.org/data/gnss/perm-sta.php.We have observed ionospheric phase scintillation in Canada, but all the rest six countries have not observed ionospheric phase scintillation in March 16(initial phase). We have also observed ionospheric phase scintillation in Canada and Italy, we have not observed ionospheric phase scintillation in Austral, Slovakia, Ukraine and Switzerland in March 17(main phase).We have observed ionospheric phase scintillation in Italy, Canada and Austria and Slavonia and Ukraine and we have not observe ionospheric phase scintillation in Swaziland in March 18(recovery phase).We have observed ionospheric phase scintillation in Italy, Austria, Canada, Slavonia, Ukraine and Swaziland in June 22(initial phase).We have observed ionospheric phase scintillation at Canada and we have not observed ionospheric phase scintillation in and we have not observed ionospheric phase scintillation in Italy, Austria, Slavonia, Ukraine and Swaziland in June 23(main phase).We have observed ionospheric phase scintillation in Italy, Canada and Swaziland and we have not observed ionospheric phase scintillation in, Austria and Slavonia were observed strong fluctuation, Ukraine in June 24(recovery phase). We have observed ionospheric phase scintillation in Slovakia and the remaining countries did not have observed ionospheric phase scintillation in December 19(initial phase) .We have observed ionospheric phase scintillation Canada and the remaining countries were not observed ionospheric phase scintillation in December 20 (main phase) .We have not observed ionospheric phase scintillation in December 21(recovery phase) observed in all station. Generally ionospheric phase scintillation dependant on longitude.

Chapter One

1. Introduction

1.1BackGround

The ionospheric irregularities are generated after sunset over the magnetic equator due to plasma instabilities and the most important parameter for their development is the equatorial evening vertical plasma drift ($\mathbf{E}\times\mathbf{B}/B^2$) known as prereversal enhancement in vertical drift, when the eastward electric field is intensified due to the action of the F-region dynamo. During magnetic storms, strong eastward (westward) electric field from the magnetosphere (disturbance dynamo) can penetrate to equatorial region intensifying (weakening) the upward plasma drift and consequently triggering (inhibiting) the ionospheric irregularities. This subject has been studied by many authors since ionospheric irregularities cause scintillation in the GPS signal amplitude and phase and can affect telecommunication systems, and magnetically quiet time scintillation pattern can be modified during storms. The storms also can affect drastically the TEC (Moldwin, 2008).

During magnetic storms, supersonic solar plasma emissions distort the magnetosphere that is a cavity formed by the interaction of the solar wind with the Earth's magnetic field. The magnetosphere has a long tail, that extends in the opposite direction to the Sun. magnetic storm occurs when a long-lasting interplanetary convection electric field leads, through a substantial energization in the magnetosphere-ionosphere system, to an intensified ring current sufficiently strong to exceed some key threshold of the quantifying storm time Dst index. Energy from the solar wind is transferred to the ionosphere-thermosphere-magnetosphere system, intensifying convection electric fields in the magnetosphere and producing an enhancement of particles precipitation, and currents in the high latitude ionosphere. During magnetically disturbed periods the magnetospheric shielding layer is not effective to shield magnetosphere electric fields which therefore penetrate directly to low latitudes The structure and dynamics of the thermosphere and ionosphere is globally affected due to the increase of ionospheric conductivity, the Joule heating and the ion drag in the upper atmosphere of high latitudes and the disturbance dynamo gives origin to westward electric field that penetrates to equatorial region that could last up to 30 hours after the end of the storm main phase(Hun and Hargreaves, 2003).

1.2 Objectives and Research Question

The objective of this research is to investigate the longitudinal variations of phase scintillation during geomagnetic storm.

Research question

- How ionospheric scintillation does behave longitudinally during geomagnetic storm?

1.3 Statement of the Problem

Ionospheric scintillation causes rapid phase and amplitude fluctuations in GPS signals. The combination of simultaneous deep fades and phase rotations creates cycle slipping in the phase locked loops that are used to achieve carrier recovery. Cycle slipping causes the tracking scheme to return an inaccurate estimate of the actual carrier frequency and in some cases, can lead to frequency unlock (Nathana, 2013). Many researchers have studied about the occurrence and effect of ionospheric scintillation on GPS signals over east Africa. But most studies do not include the variation of ionospheric scintillation with longitude. The influence of geomagnetic storms on plasma irregularities is studied by its effect on the upward E X B plasma drift. The storm induced electric fields can either enhance or cancel the local eastward electric field thereby triggering or inhibiting ionospheric irregularities which causes signal fading (Ephrem & Melessew, 2016).The characteristic of ionospheric scintillation was studied by (Taabu et al., 2016). They showed that ionospheric scintillation is a post-sunset phenomenon at Bahir Dar station. GPS signal becomes weakened or scintillated when it passes through electron-dense regions, where the irregular electron-dense regions that cause scintillation are small scale rather than large scale. The scintillation index also depends on the satellite elevation angle. The contribution of magnetospheric currents to ground magnetic perturbation during geomagnetic storms was studied by (Swadesh, 2013). Characterizations of ionospheric scintillation at geomagnetic equatorial region station was studied by (Ephrem & Tsegaye, 2015). They concentrated on a specific area or a country and different latitude but in the same longitude. longitudinal or west to east variation of phase scintillation was not studied east African selected station during geomagnetic storm. So that this am to study the longitudinal variation of phase scintillation in two different continents including the seven countries during geomagnetic storm in March (16-18), June (22-23) and December (19-21) in the year of 2015.

1.4 Significance of the Study

This title is very important essential and un interesting topic. This research is important for understanding of ionospheric scintillation, ionospheric irregularities, the phase scintillation of ionoephere, *total* electron content, global position system in the ionospheric scintillation etc for all master student, phD student, and all natural since and computiitional since student. The important of the study is that to know characteristics phase scintillation the longitudinal in Canada and Europe.

1.5 Organizations of this Thesis

Chapter 2 an introduction ionospheric scintillation, layer of earth atmosphere and neutral atmospheres, the ionosphere, *The Ionosphere* , Structure and Regions of Ionosphere , *Major geographic regions of the ionosphere* , Morphology of Scintillation , ionospheric irregularity, E-region Irregularities , F-region Irregularities , Geomagnetic Storms and Their Ionospheric Effect , Geomagnetic Storms , Ionospheric Disturbances , Ionospheric Storm and Space Weather , geomagnetic storm, solar wind variation, and geomagnetic storms and magnetic indices.

Chapter 3 This chapter overviews on data source, data analysis, and ionospheric total electron content.

Chapter 4 This chapter presents the main output or the objective of the study. Longitudinal dependency of Ionospheric Scintillation during Geomagnetic Storm, Variations of VTEC, ROT and ROTI during Geomagnetic storm in March (16, 17 and 18), 2015, Variations of VECT, ROT and ROTI during geomagnetic storm on June 22, 23 and 24, 2015, Variations of VECT, ROT and ROTI during geomagnetic storm on December (days:19, 20 and 21, 2015, and the results, discussions and summary of the studies are discussed.

Chapter Two

2. Literature Review

This chapter is divided into three main sections. In Section 2.1. Ionospheric scintillations**,** 2.2 ionospheric irregularities**,** 2.3 Geomagnetic storms and their ionospheric effect, to be in this thesis are identified.

2.1. Ionospheric Scintillations

The Ionospheric scintillation is a rapid random fluctuation of radio-frequency signal phase and/or amplitude, regulated by signal passes through the ionosphere, when a plane wave traverses a region of small scale irregularities in electron density. Due to a small fluctuation in refractive index of a medium of the signals, the ionospheric irregularities lead to skew (bend) the signals path, which depends on the differential of electrons; consequently, the scintillation is occurred. In case of signal frequency beyond 3 GH only tropospheric scintillation due to atmospheric turbulence along the propagation can occur, and which results degradation of signal (Jiao et al., 2015) . Such effects arise from radio frequency propagation through regions where small-scale irregularities in electron density exist. These regions can range in size from a few meters to a few kilometres, and they cause both refraction and diffraction of EM waves propagating through the ionosphere (Jiao et al., 2015).Ionospheric scintillation causes rapid phase and amplitude fluctuations in GPS signals. Scintillation is caused by small-scale fluctuations in the refractive index of the ionospheric medium which in turn are the result of in homogeneities. In homogeneities in the ionospheric medium are produced by a wide range of phenomena (eg plasma bubbles), and those responsible for scintillation occur predominantly in the F-layer of the ionosphere at altitudes between 200 and 1000km (Jiao et al., 2015). In addition to that the scintillation may occur in different phenomena, scintillation occurred with time variation, location variation, and geomagnetic variation. Since the equatorial ionosphere is highly dynamical, unpredictable and is characterized by the existence of intense equatorial plasma bubble associated irregularities; during low and moderate solar activity, the occurrence pattern of equatorial ionospheric irregularities varies with local time and that only the occurrence probability of irregularities based on plasma density perturbations is consistent with the occurrence of scintillation at all local times. Equatorial plasma bubbles (EPBs) has a significant role as source of ionospheric radio wave scintillation that can cause disruptions and outages of

important radio-related information such as GPS Systems and ground-to-satellite radio communication.

2.1.1 Layers of Earth Atmosphere and Neutral Atmospheric Layers

The Earth's atmosphere is an envelope of thin gas that surrounds the Earth and extends from the Earth's surface out thousands of kilometres, becoming increasingly thinner (less dense) with distance but always held in place by Earth's gravitational pull. The atmosphere contains the air we breathe and it holds clouds of moisture (water vapor) that become the water we drink. It protects us from meteors and harmful solar radiation and warms the Earth's surface by heat retention. In effect, the atmosphere is an envelope that protects all life on Earth (Hun and Hargreaves, 2003).

The atmosphere is a mixture of gases we call "air" (Moldwin, 2008). On a dry volume basis, it consists of about 78% nitrogen and 21% oxygen. The remainder of about 1% contains argon, carbon dioxide and very small amounts of other gases. The atmosphere is rarely, if ever, completely dry. Water vapour is almost always present up to about 4% of the total volume. In desert regions, when dry winds are blowing, water vapor in the air will be nearly zero

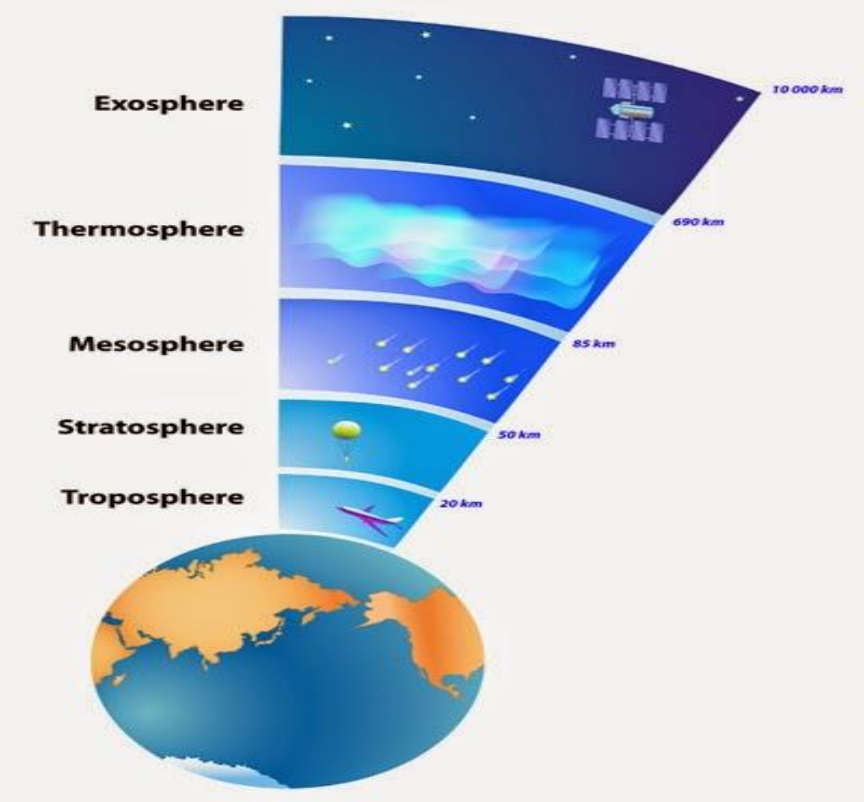

Figure 2. 1Vertical profile of the neutral atmosphere or Layers of Earth's atmosphere from the lower Troposphere to upper Exosphere (from Bishop, et al., 1991).

This climbs in other regions to about 3% on extremely hot and humid days. The upper limit, approaching 4%, is for tropical areas. The atmosphere has a total mass of about metric tons and about 80% of that mass is within about 12 kilometres from the Earth's surface. There is no definite boundary between the atmosphere and outer space. It slowly becomes less dense (i.e., more empty) and fades into the void of outer space (Kallenrode, 2004).

Generally, Atmosphere is the collection of different atoms and molecules. It encloses the Earth. Figure 2. 2 show that the earth's atmosphere layers ordered from lowest to the highest layer, as the Troposphere, Stratosphere, Mesosphere, Thermosphere and the Exosphere. There are four boundaries between the primary layers, referred to as Tropopause, Start pause, Menopause and the Thermo pause.

2.1.2. The Ionosphere

As you know, when you climb up a high mountain, the atmospheric pressure and temperature decrease with altitude. However, the temperature does not monotonically decrease with altitude because ultraviolet (UV) radiation from the sun is absorbed in specific regions in the atmosphere. One is an ozone layer in the stratosphere, and the other is an ionosphere at the top of the atmosphere (50-1000km) (Amensisa et al., 2015). In this region, the atmospheric particles are partially ionized, so that HF radio wave can be reflected to travel long distance (Moldwin, 2008). The ionosphere is a transition region from Earth's atmosphere to the space, in other words, the entrance to the outer space **Error! Reference source not found.**. The ionosphere, a part of the Earth's upper atmosphere, contains partially ionized plasma that is continuously changing under the influence of extreme ultra violet (EUV) radiation, recombination, neutral winds and electric field. The ionosphere has sufficient electron content to support terrestrial communication up to high frequency (HF) and can disturb the trans-ionospheric communication. It extends from a height of above 50 km and overlaps the ozonosphere to over 1000 km. Ionospheric plasma is non-homogenous, anisotropic, and dispersive, weakly ionized, magnetized, cold and colissional. Peak electron densities in the ionosphere vary greatly with time (diurnal, seasonal and sunspot cycle), geographic location (polar, auroral zones, mid latitudes and equatorial regions), and certain solar related ionospheric disturbances (Hun and Hargreaves, 2003).

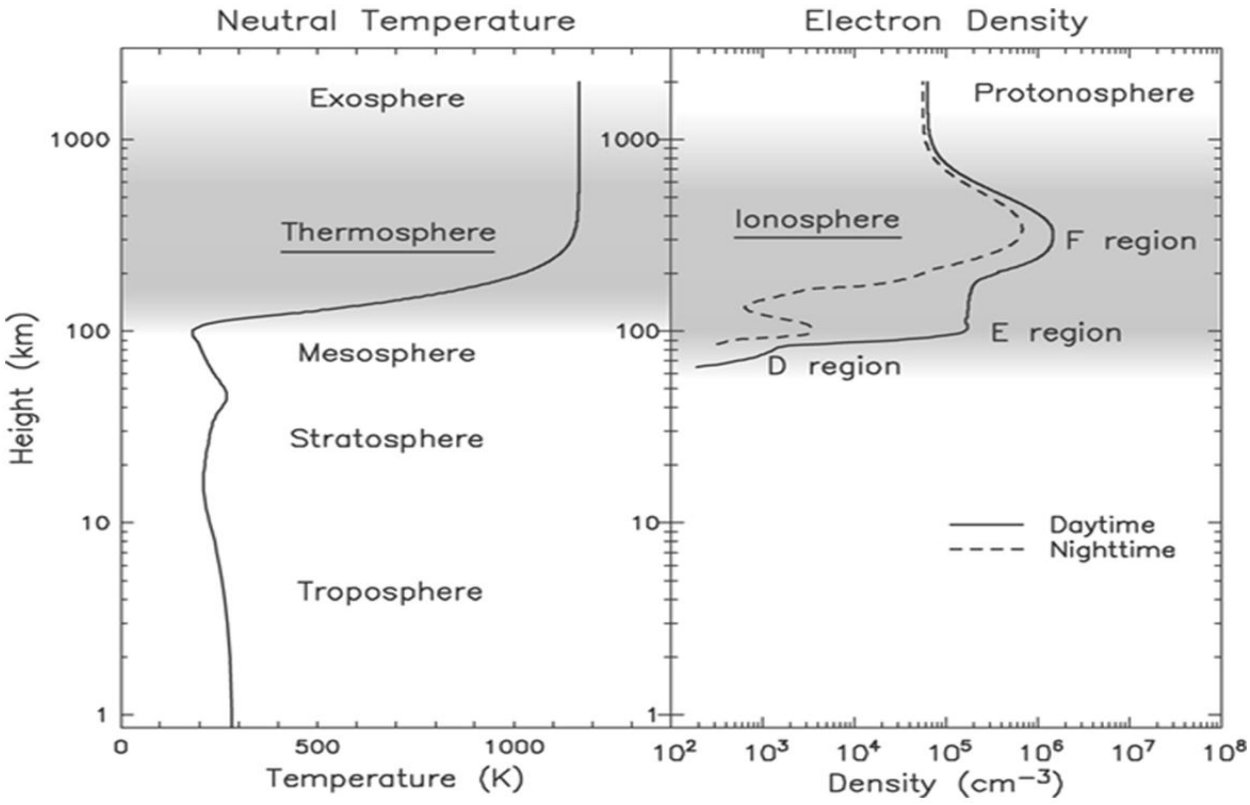

Figure 2. 3: Atmospheric structure from ground to space [Australian Space Weather Agency, 2011]

2.1.3. Structure and Regions of Ionosphere

Based on the electron density profile, the ionosphere is divided into D, E, F-regions which occupy the heights varying approximately from 70-90 km, 90-150 km, and 150- 1000 or so km respectively. The F-layer is further divided into F1- (150-210 km) and F2- (over 210 km) layers during the daytime. The typical electron density structure of day and night time ionosphere is shown in **Error! Reference source not found.**.

D-region: This region is only present in the day and are the lower most layers extending from 50-90 km from the surface of the Earth. The quiet time D-region is produced by the photo-ionization of NO by the most penetrating Lyman α radiation at a wavelength of 121.5 nm. During active phase of solar activity with 50 or more sunspots, hard X-rays with wavelength < 1 nm ionizes the air (N2, O2). During the night time, cosmic rays produce ionization and the electron density of this region varies from 10^8-10^9 m^{-3}. High energy electron precipitation is a source of D-region ionization in the auroral region (Briekke, 2013). High frequencies (HF = 3-30 MHz) pass through this layer, while the low frequency waves (LF = 30-300 kHz) are absorbed by this layer. The absorption is due to the layer being weakly ionized and having a very high ion-neutral collision frequency. Extremely low

frequency (ELF = 3 Hz-3 kHz) and very low frequency (VLF = 3-30 kHz) are reflected and also partially absorbed by the D-region (Schunck & Nagy, 2009).

***E-region**:* The E-region extends from 90-150 km and undergoes a large day to- night variations. This has daytime electron density of about 10^{11} m^{-3}. The E-region remains throughout the night with decreased electron density of about 5×10^{9} m^{-3}. The most extensively found positive ions in this region are O^{2+} and NO^{+} that are produced by the X-rays with wavelength of 1-10 nm and the UV radiation. In this region strong electric currents are generated by the dynamo effect. It reflects radio waves with frequencies less than about 10 MHz and deteriorates the signals above 10 MHz as it partially absorbs these waves (Hun and Hargreaves, 2003).

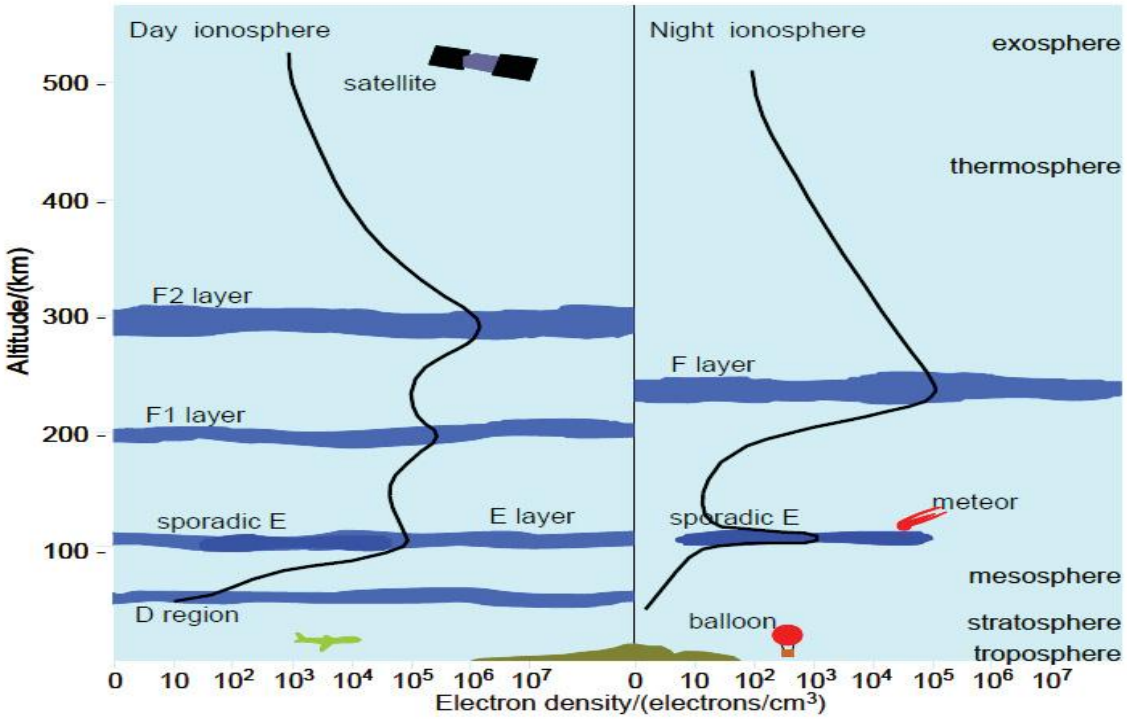

Figure 2. 4:Day and night structure of the ionosphere [Australian Space Weather Agency, 2011]

***F-region**:* Above the E-region lies the F-region. The plasma density in the F region increases with altitude up to about 300 km and then decreases. The electron density in this region is in order of 10^{12} m^{-3} in F peak. The F region splits into F_1 and F_2 regions during the daytime. The F-region plays a vital role in the High frequency (HF) communications since it contains the largest concentration of electrons. The dominant ion is O^{+}. At daytime, the F_1 layer is able to reflect radio waves up to wavelengths of about 30 m. The F_2 layer is characterized by having large electron density with a maximum approximately at 300-400 km altitude. Therefore, F layer engenders the largest effect on trans-ionospheric communications. However, a few

hours after the sunset, the F1-region becomes very much depleted and the F_1 and F_2 layers merge to form the F layer in the night time. This condition of high density plasma on top of low density plasma is very unsteady and if the equilibrium is disturbed, then irregularities are generated.

2.1.4 Major geographic regions of the ionosphere

Generally, the terrestrial ionosphere has three major geographical regions, namely the equatorial, the mid latitude, and the high latitude regions. The identification of these regions is based on the rather different properties according to their geomagnetic latitude. In the following sub section, the main characteristics of these three regions are illustrated (Figure 2.4) and described (Papagiannis, 1972).

The equatorial region: The equatorial region of the ionosphere, occasionally referred to as the low latitude zone, extends to 20°-30° on either side of magnetic equator. It is strongly influenced by electromagnetic (EM) forces that arise due to the geomagnetic field which runs horizontally over the magnetic equator. This region is known for the high values of peak electron density with the utmost prominent amplitude and phase scintillation effects. Combining the effects of the high radiation level from the Sun and electric and magnetic fields of the Earth result in electrons rising up due to a horizontal electric field produced by the dynamic action in the E-region, and then moving along the horizontal lines of the magnetic field. The electrons will drift due to a combination of thermal diffusion and electrodynamic drift along the magnetic field lines to higher geomagnetic latitudes, causing a high concentration of electrons, termed ionospheric equatorial anomalies (IEA). This phenomenon, known as the fountain effect, results in the distortion of the general form of the ionosphere throughout the low latitude zone.

The mid-latitude region: The mid latitude region is roughly between 35°-65° latitude in the north and the south, and is occasionally referred to as the temperate region. It is the region that has been explored the most completely and is best understood. This region has the smallest amount of variability and is the most undisturbed among the different ionospheric regions. In this region the ionization is almost entirely influenced by energetic solar EUV and X-ray emissions from the Sun, which result in ionization of the daytime ionosphere. Night-time ionization results from chemical recombination processes, which involve neutral atmosphere in addition to ionized species. The majority of ionospheric observations and studies have been done over this region, due to the fact that the majority of ionosphere sensing instruments have been established in countries situated in the mid-latitude region.

The high latitude region: In the equatorial region, a strong current flow in the E-region and the F-region is subject to electrodynamics lifting and the fountain effect. At high latitudes, the situation is totally opposite. In this region, the geomagnetic field runs virtually vertical, and this change leads to the existence of an ionosphere that is greatly more complex than that in the mid and low latitude zones. Motivation for this complex change is because the magnetic field lines connect the high latitudes to the outer part of the magnetosphere, which is determined by the solar wind and eventually leads to the charged particles descending to E layer altitudes (Jiao et al., 2015).

However, whereas the ionosphere at mid latitude zones is linked to inner magnetosphere, which basically rotates with the Earth and is thus less responsive to external influence (Hun sucker and Hargreaves, 2003), the high latitude region is dynamic and thus circulates in a pattern that is primarily controlled by the solar wind but is also variable. Energetic particle emissions from the Sun are easily accessible in this region, which produces additional ionization, and thus this region can be affected by sporadic events that can degrade polar radio propagation. When these energetic particles collide with neutral atmospheric gases, local enhancements of electron densities result, as for example during auroral activity.

Auroral activity involves interactions between the magnetosphere, the ionosphere and the atmosphere. Auroral zones occur within the high latitude region, and their location depends on the linkage with the magnetosphere. Characteristically auroral zones are relatively narrow rings located in the higher southern and northern geomagnetic latitudes. In general, the intensity and the position of the auroral oval results from the linkage with the magnetosphere and is related to geomagnetic perturbations. Auroral phenomenon includes electro jets, which causes magnetic perturbations and also sub storms, where the rate of ionization increases greatly due to the arrival of energetic electrons. These auroral zones are regions that are particularly complex for radio propagation. The geographical regions enclosed by the auroral rings are called the polar caps, and these regions are affected tremendously by solar flares and Coronal Mass Ejections (CME) causing the D region electron density enhancements (Schunk et al., 2000).

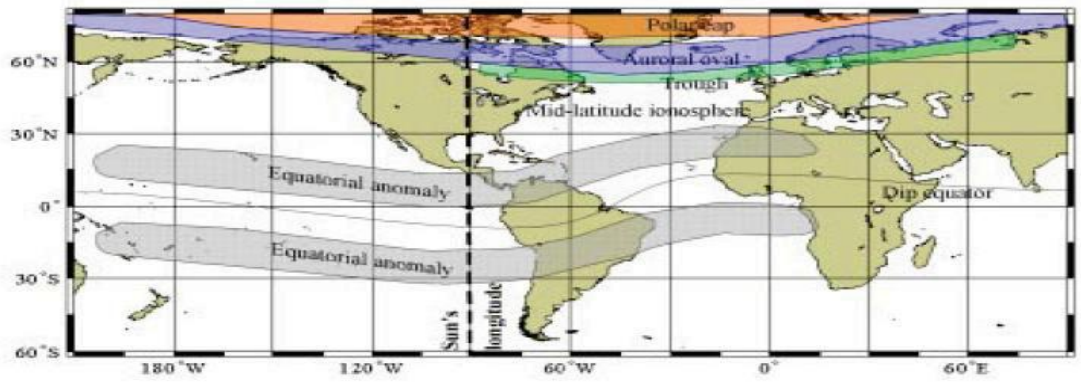

Figure 2. 5: Geographic regions of terrestrial ionosphere (from Bishop, et al., 1991).

2.2. Morphology of Scintillation

Ionospheric scintillations are categorized into amplitude scintillations and phase scintillations. The processes that produce scintillations in these two regions are quite different, leading to significant differences in the characteristics of the resulting scintillations. Auroral and polar cap scintillations are mainly the result of geomagnetic storms 1 that are associated with solar flares 2 and coronal holes 3. Unlike equatorial scintillations, they show little diurnal variation in their rate of occurrence, and can last from a few hours to many days, beginning at any time during the day (Guo et al., 2016). Large and rapid variations in the plasma density are often associated with auroral and polar cap scintillations and can lead to significant errors in differential GPS (DGPS) systems as well as rapid changes in the apparent range and range rate. Auroral scintillations also show a seasonal dependence which is the reverse of that observed at low latitudes, being greatest from the autumn equinox through winter to the spring equinox, and a minimum during the summer months. Indeed, the geomagnetic disturbances that excite auroral and polar cap scintillations tend to suppress the onset of equatorial scintillations during solar maximum periods. Because geomagnetic storm activity is linked to solar activity through solar flares and coronal holes, auroral and polar cap scintillations also show a strong dependence on the 11-year solar cycle, being most intense during solar maximum periods, but almost non-existent during minima. Scintillations are mainly confined to the equatorial and polar regions. Equatorial scintillations, on the other hand, are produced by irregularities in the F-layer of the equatorial ionosphere following the passage of the evening terminator1 and tend to disappear soon after midnight. In these regions, the most severe scintillations are associated with the crests of the equatorial anomaly which are centred approximately 15° either side of the magnetic equator. As equatorial scintillations are coupled to the anomaly, they tend to be worse during the years of solar

maximum when the anomaly is at its greatest. During the seasons of high scintillation activity, the equinoctial months of March and September tend to suffer the highest levels of activity, although this does not appear to be true at all longitudes (Kallenrode, 2004).

Equatorial scintillations are mainly produced by irregularities created by instabilities in the F-layer of the ionosphere during the evening hours. After sunset, the lower regions of the F-layer recombine more rapidly than the upper regions, leading to an unstable situation akin to a heavy fluid being supported on a lighter fluid2. This situation eventually leads to the formation of bubbles of low density plasma which are forced upwards through the denser upper regions. As the bubbles grow, steep density gradients on the walls cause smaller irregularities to form. At GPS frequencies, these smaller irregularities, which can be of the order of the Fresnel zone radius or less (< 300m), are responsible for scintillations. The low density bubbles eventually form into irregularity patches, or *Plumes*, which can reach heights of up to 1500km at the magnetic equator. Once formed, the plumes extend along the magnetic field lines in a North-South direction for over 2000km, leading to an accumulation of irregularities in the Northern and Southern anomaly regions (±150 to ±200 dip latitudes3). Because of the higher background densities in these regions, the irregularities tend to produce much stronger scintillation effects than at the magnetic equator. Irregularity plumes typically have East- West extents of between one and several hundred km's and tend to move in an Easterly direction with velocities of the order of 50 to 200 m/s (Jiao et al., 2015). Consequently, scintillations are often experienced in patches that can last for an hour or so with periods of little or no activity in between. Eventually, in the absence of solar radiation, the irregularities begin to fade along with the associated scintillation activity. This usually occurs around local midnight, although at times scintillations can persist until early morning.

Scintillations can also occur during daylight hours and at mid-latitudes when Sporadic-E is present in the E-layer. Sporadic-E is thin layers of highly dense plasma at heights of about 100km in which large density gradients can exist. However, scintillations produced by Sporadic-E are much less common and less predictable than those produced by the F-layer processes described above (Ratclffe, 2004).

2.3 Ionospheric Irregularities

Plasma instabilities and other magnetospheric sources may generate fluctuations in electron densities that are called "ionospheric irregularities". The irregularities may disturb a traversing radio signal leading to distortion of its phase and amplitude. These signal distortions, as observed from the ground, are known as ionospheric scintillations.

Scintillations are frequently observed in high latitude and equatorial regions. The occurrence of scintillations is also dependent on the phase of the solar cycle, the season, and the time of the day. Global Positioning System (GPS) signals can suffer fading, and GPS receivers may even lose lock on the signal due to ionospheric scintillations. In this thesis ionospheric scintillation is briefly explained in 2.1. As described shortly, ionospheric irregularities have been studied extensively in low latitude regions. The high latitude irregularities on the other hand are dynamic and largely unexplored. The nearly worldwide availability of GPS signals, especially in high latitudes with recent development in dual frequency GPS receivers enables us to utilize scintillation induced GPS signal variations in the study of high latitude irregularities (Michael et al., 2009).The ionospheric plasma is non-homogenous, dynamic, and in continuous motion as a result of neutral winds and electric field. In addition, the plasma in space is also not in its thermo-equilibrium state, so in order to come to a true equilibrium, the plasma needs to shed some of its energy to some wave modes. In doing so, the amplitude of the plasma grows with time and this growing plasma wave is called an unstable mode. In other words, the plasma instability is a process whereby the free energy of the plasma gets converted into a growing mode in a collective way. These instabilities create fluctuations and structures in the plasma density which is known as irregularity. The irregularities are found at all latitudes of the globe with scale sizes varying from centimetres to kilometres. The ionospheric irregularities have been clustered into E- and F-region instabilities or irregularities.

2.3.1 E-region Irregularities

The E-region irregularities are commonly known as Sporadic- E layer or Es. The Es is characterized by a thin reflecting layer in the ionosphere which comes and goes sporadically at E-region altitudes of 100-120 km where the ion motion is controlled mainly by collisions with neutrals. Es usually consists of metallic ions. Weaker forms of Es consist of cloud of ionization and the most intense forms consist of a thin sheet of ionization some tens or hundreds of meters in thickness which can vary from 0.5-5 km and the horizontal extent can vary from 10-1000 km. Es is observed on ionograms as an echo at constant height which extends to a higher frequency than usual critical of the E-region.

The Es is observed at all the latitudes, however, the strongest and more frequent layers occur at the mid-latitudes since the two ion convergence mechanisms (zonal wind shear and meridional wind shear) does not work efficiently at the magnetic equator and in the auroral zones. Es occurs through the mechanism of wind shear theory, whereby the East-West winds

in the E-region causes a vertical movement, compressing the ions into thin layers of high density. The wind shear theory, proposed by Whitehead relies on the process of vertical shear in the horizontal wind which in the presence of Earth's magnetic field forms a layer of ionization, the Es. The ionosphere over equatorial and low latitudes is very strongly influenced by the Earth's magnetic field.

Usually, it is more useful to consider how the ionosphere varies with geomagnetic latitude or with dip angle of the Earth's magnetic field rather than within a geographic framework. Es formed in the equatorial region is known as the Equatorial Sporadic-E (Esq). Esq has been found to be formed due to plasma instability caused by the high electron drift velocity associated with Equatorial Electro jet (EEJ) and is present during both day and night even when the electron densities are greatly reduced.

Generally, Es appears as patchy and mostly transparent region, while sometime it appears in sheet which can completely cover the overlying F-region. Radar spectral studies have revealed two distinct types of irregularities; Type I and Type II. Type I occurs only when the electro jet current exceeds some minimum value. These irregularities travel with a phase velocity equal to the ion-acoustic speed and are thought to be generated by the excitation of the two stream instability.

The Type I irregularities propagate perpendicular to the Earth's magnetic field at the ion acoustic velocity. Type II irregularities are generated by the gradient drift instability and are found to propagate smaller than the ion-acoustic speed. Type II irregularity also known as cross field or **E×B** instability because of cross **E** and **B** form the driving forces. These irregularities are practically always present both during the day and the night, even when type I irregularities are absented since, Type II irregularities emerge when the electron drift is insufficient to produce type I irregularities.

During the day time the large conductivity of the E-region prevents the growth of equatorial F-region of plasma instabilities by short-circuiting any perturbation electric field associated with plasma wave, however, soon after sunset, these F-region irregularities become visible.

2.3.2 F-region Irregularities

The other types of irregularities that have been of great scientific interest are the F-region irregularities. Plasma bubbles or plumes are the terms used to describe the F-region irregularities and were initially reported in 1950's. Since then a number of techniques have been used to study these irregularities, such as the topside and bottom-side ionosonde, radio-

star scintillations, VHF-backscatter radar, Langmuir probes on board satellites and the GPS scintillations (Michael et al., 2009).

The F-region irregularities are associated with equatorial Spread-F (ESF) and can be expected at all latitudes. Spread-F generally remains confined around the geomagnetic equator which is 20° on either side of the dip equator. Instabilities can occur in the post-sunset hours at the equatorial latitude of the F-region of the ionosphere. It is now accepted that the ESF occurs at the bottom of the F-region due to the Gravitational Rayleigh-Taylor (GRT) instability.

GRT as the physical mechanism for the growth of equatorial plasma bubbles (EPBs). The condition for GRT develops after sunset at the geomagnetic equator when the bottom-side of the F-layer recombines with the dense neutral atmosphere. Simultaneously, the pre-reversal enhancement raises the F-region to higher altitude. As a result, a sharp vertical gradient in electron density exists. This condition of high density plasma on top of low density plasma is very unstable. Using the analogy of fluid dynamics, it could be modeled by having a less dense fluid supporting a high-density fluid, on top, against the gravity. In here, it is the high-density F-region (representing the heavy fluid) supported on the lesser dense one by the magnetic field.

Consequently, a lump of the low-density layer raises causing density irregularities known as equatorial plasma bubbles (EPBs). The growth rate of the GRT instability depends on the density gradient. The gradient becomes steeper after sunset (Michael et al., 2009).The EPBs are generated after sunset at the magnetic equator. Due to GRT instability, the EPBs rise to higher altitudes and then travel to higher latitudes due to non-linear evolution of the $\mathbf{E}\times\mathbf{B}$ drift. Dungy in 1956 originally proposed the idea of GRT instability. When fully grown these irregularities contain a wide range of scale sizes which have been detected by ground based radio sounders, night airglow measurements, satellite measurements and backscatter radar echoes. Studies have shown that ESF occurs more often in the equatorial region which appears to be closely related to the increase in the height of the F-layer at the low latitudes (Hun and Hargreaves, 2003).

Ionospheric irregularities have also been classified into different categories according to their scale sizes; Planetary (> 1000 km), Medium Scale (10-100 km), Intermediate Scale (0.1 10km), Transitional Scale (10-100 m), and the Short Wavelength Scale (< 10 m). The tendency of these irregularities to interfere with trans-ionospheric communication is quite high. Plasma irregularities cause rapid fluctuations known as scintillations in phase and hence amplitude of signals passing through the ionosphere. Daytime random scintillations occur due

to Sporadic E-layer and the night-time predominantly due to the ESF in the low and equatorial latitudes.

2.4 Geomagnetic Storms and Their Ionospheric Effect

The studies of magnetic storm effects on the ionosphere usually concentrate on the deviation of the F-layer parameters during storm periods from monthly averages (Sahai et al., 2007) .Effects of electromagnetic drift can be studied by changes in the height of the F-layer . Danilov and Morozova suggested the characteristics of ionospheric storms should be studied in terms of deviations of the F-layer critical frequency foF2 for positive and negative phases from the median value and changes in the minimum virtual height HF and the peak height F2 (Kallenrode, 2004).

2.4.1 Geomagnetic Storms

Geomagnetic storms are strong disturbances in the Earth's magnetosphere due to changes in the solar wind and interplanetary magnetic field (IMF). It is a temporary disturbance of the Earth's magnetosphere caused by transfer of energy and momentum from a solar wind shock wave and/or cloud of magnetic field which interacts with the Earth's magnetic field (S.Aschwaden, 2004) . The increase in the solar wind pressure initially compresses the magnetosphere and the solar wind's magnetic field interacts with the Earth's magnetic field and transfers an increased energy into the magneto sphere. Both interactions cause an increase in movement of plasma through the magnetosphere (driven by increased electric fields inside the magnetosphere) and an increase in electric current in the magnetosphere and ionosphere.

The ionospheric response to a geomagnetic storm, which is commonly referred to as an ionospheric storm, is not yet completely understood and remains one of the primary subjects of ionospheric science. An ionospheric storm is a global phenomenon; it extends to all latitudinal regions and both dayside and night side hemispheres of the Earth, and affects all branches of telecommunication and navigation. Geomagnetic disturbances begin with the arrival of solar/interplanetary plasma at high velocity at Earth's magnetopause.

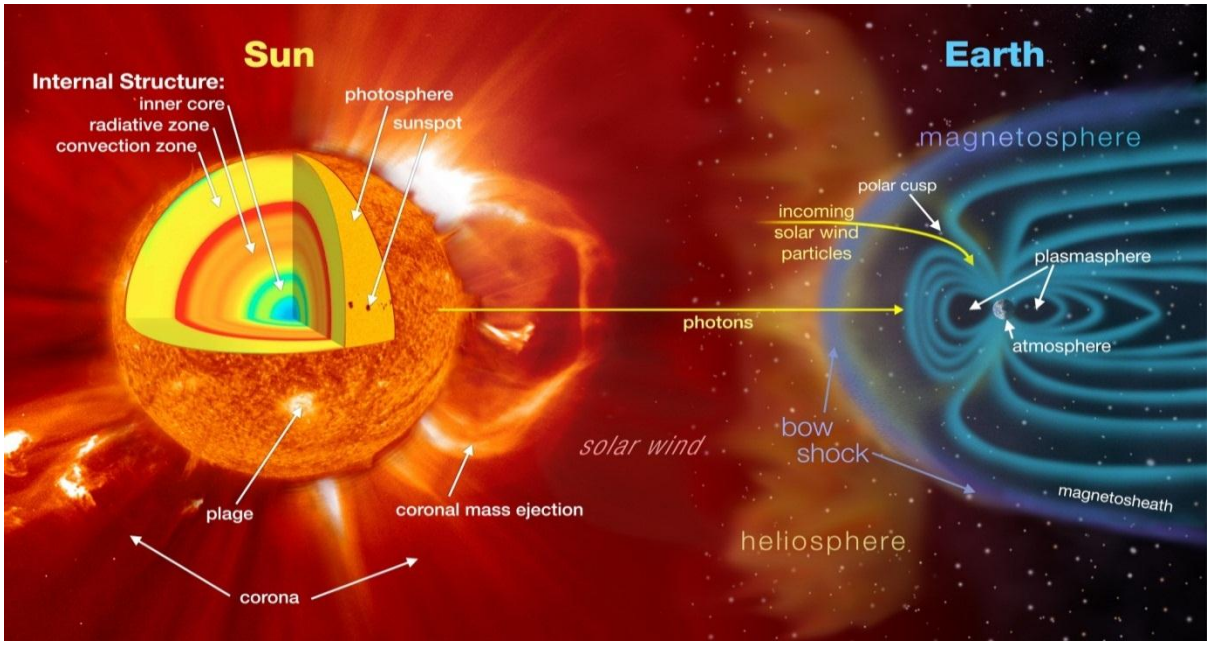

Figure 2. 6: Artist's depiction of solar wind particles interacting with Earth's magnetosphere. Sizes are not to scale Bishop, 1991).

The most significant geomagnetic and ionospheric effects are caused by hot plasma with a negative IMF Bz component, which sets up interconnection with Earth's magnetic field lines and leads to a large amount of energy deposition into the high-latitude regions of the Earth. Such high-latitude heating, in turn, can create strong dawn-to-dusk disturbance dynamo electric fields. From the figure above **Error! Reference source not found.** show that the disturbance of magnetosphere.

The major phases of typical geomagnetic storm are shown in **Error! Reference source not found.** and can be described as follows,

- Sudden storm commencement (SSC) is characterized in low and mid-latitudes by an increase in H is typically 20-30 nT Occasionally it can be as much as 50-100 nT The increase in H is largest at equatorial stations and has a rise time of 1 to 6 minutes. SSC is the signature of the magnetopause current generated due to the compression of the magnetosphere when shock arrives and superposition of other transient magnetospheric and ionospheric currents. However, each storm might not be accompanied by SSC.
- Initial phase follows SSC and it is the period during which H is above the storm pre-onset value. The initial phase typically lasts for 0-8 hours. This phase is due to the increased pressure of the solar wind on the geomagnetic field associated with the increase in density and speed at and behind the shock. This continues until the diffusion of plasma (trapping of protons) in the geomagnetic field becomes important.

Not all storms will show initial phase which is evident in later chapters showing SYMH index during storms. An increase of magnetic field lasting a few hours only.

- Main phase is a period following the initial phase during which H falls below its initial undisturbed value. During this time, interplanetary magnetic field (IMF) remains southward. The main-phase decrease of -50 to - 600 nT may be taken as a typical figure though larger decrease occurs in intense storms. The main phase of a geomagnetic storm lasts for 12 - 24 hours. Often positive and negative excursions with amplitudes of the order of several hundred gammas having periods of about 0.5 hours observed in the H component. A large decrease in the H component building up to a maximum in about a day, the main phase.
- Recovery phase follows the main-phase; it starts when IMF turns northward and consists usually of slow relaxation of H back to undisturbed value with characteristic time of about one day, although a 20-30-day recovery time is also observed. The internal processes in the magnetosphere have a significant role to play in the duration of the recovery phase. A slow recovery to normal over the next few days, the recovery phase.

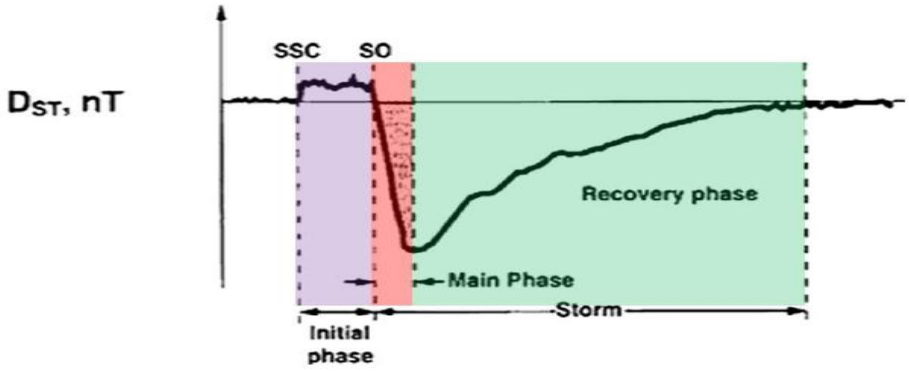

Figure 2. 7: Typical temporal profile of geomagnetic storm observed in Dst index withVarious phases (adopted from [Tsurutani, 2000])

During the main phase of a geomagnetic storm, electric current in the magnetosphere creates a magnetic force which pushes out the boundary between the magnetosphere and the solar wind. The disturbance in the interplanetary medium which drives the geomagnetic storm may be due to a solar coronal mass ejection (CME) or a high-speed stream (co-rotating interaction region or CIR) of the solar wind originating from a region of weak magnetic field on the Sun's surface. The frequency of geomagnetic storms increases and decreases with the sun spot cycle. CME driven storms are more common during the maximum of the solar cycle and CIR driven storms are more common during the minimum of the solar cycle. Generally

geomagnetic storm causes ionospheric disturbance. Ionospheric disturbance leads to ionospheric irregularities (Sahai et al., 2003).

2.4. 2 Ionospheric Disturbances

It can result from solar disturbances that occur on the Sun, and from geomagnetic disturbances, which are triggered in more complex ways by events initiating from the Sun. These events affect the outermost geomagnetic field lines and compress the geomagnetic field causing geomagnetic disturbances. Thus, the set of ionospheric disturbances is associated either directly or indirectly with events on the Sun. The ionospheric disturbance may stay for a few hours to a few days and tend to occur during times of geophysical disturbance resulting from increases in solar activity communicated via the solar wind. It can result from solar disturbances that occur on the Sun, and from geomagnetic disturbances, which are triggered in more complex ways by events initiating from the Sun. These events affect the outermost geomagnetic field lines and compress the geomagnetic field causing geomagnetic disturbances. Thus, the set of ionospheric disturbances is associated either directly or indirectly with events on the Sun (Kallenrode, 2004).

Ionospheric storms: Solar fares or coronal mass ejection (CME) result in the enhanced flux of intense energetic particles emitted by the Sun. These enhanced flux releases often generate enormous variations in the particle and electromagnetic radiation incident upon Earth and such variations can result in disturbances of the quiet time magnetosphere and ionosphere. The disturbances of the ionosphere are identified as ionospheric storms, which have a tendency to produce large disturbances in ionospheric density distribution and total electron content. These storms symbolize an extreme form of space weather, which has social and technological impacts on space borne and ground based technological systems. Like geomagnetic storm, this classical ionospheric storm consists of three phases. These phase of ionospheric disturbances (F-layer) are; initial phase or positive phase which lasts for a few hours, the electron density and the electron content are greater than normal; main or negative phase when these quantities are reduced below normal values; and recovery phase is the last event of the whole storm. The most likely cause of the main phase is abnormal heating at high latitude, which also alters the pattern of circulation of the thermospheric wind. The heating reduces the ratio [O]/ [N2] at given height in the F region, and the molecularly enriched air is then convicted down to the middle latitudes by the changed air circulation.

2.4.3 Ionospheric Storm and Space Weather

Plasma density in the ionosphere is determined by the product of neutral atmospheric density (pressure) and the UV radiation intensity. Because the atmospheric density decreases and the UV radiation increase with altitude, the plasma density has a peak at altitudes of 300-400 km where many satellites such as International Space Station are orbiting. Radio waves transmitted from satellites at much higher altitudes such as GPS satellites must propagate through the ionosphere before reaching the ground. When the ionosphere is under disturbed condition, it may degrade the amplitude and phase of the radio waves and cause severe error in GPS signals (**Error! Reference source not found.**). Therefore, it is very important to monitor and understand the ionospheric condition continuously (Kallenrode, 2004).

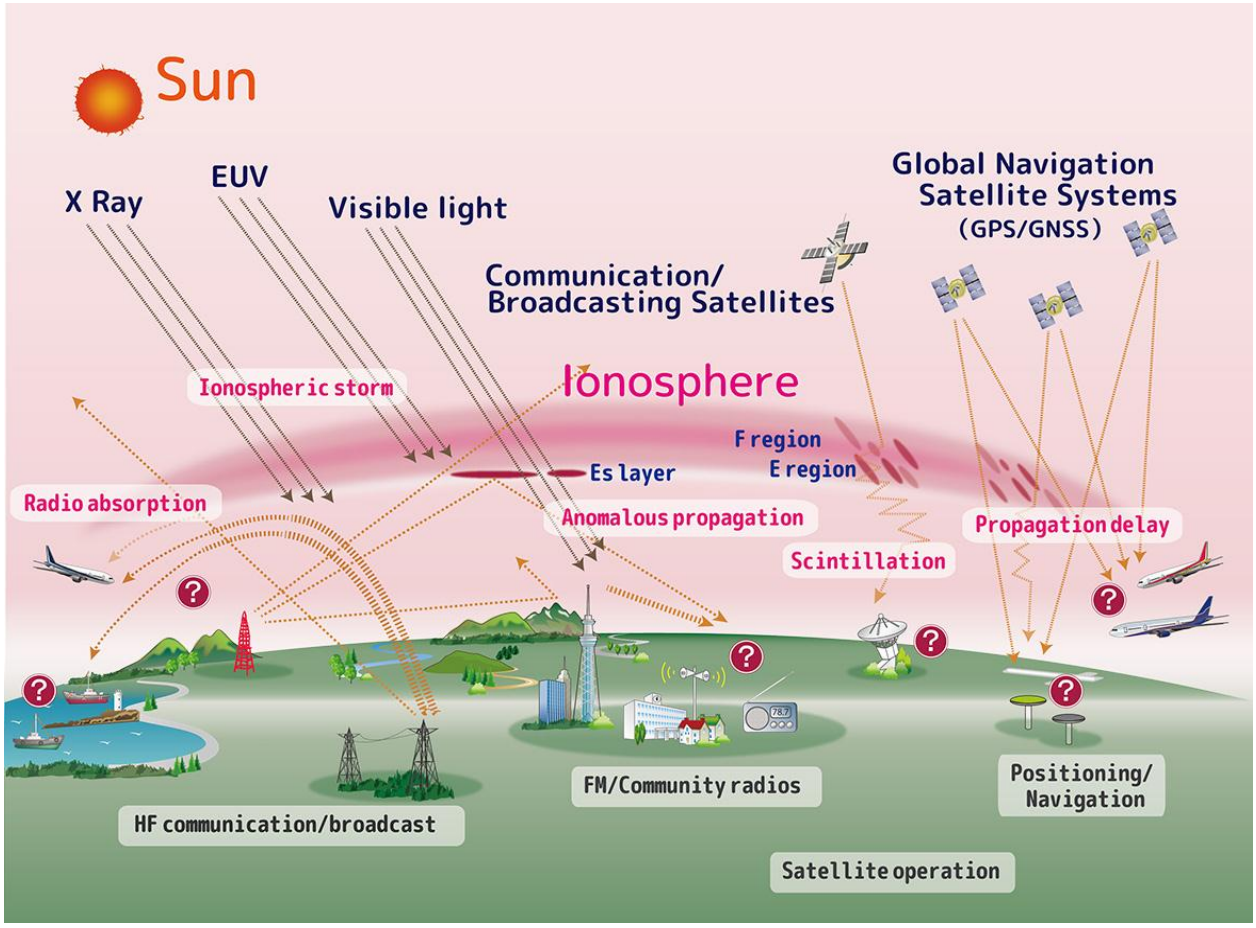

Figure 2. 8: Ionospheric effect on radio propagation (Gao and Liu, 2002).

Plasma density in the ionosphere is horizontally stratified under the quiet condition. The vertical structure and seasonal/local time variations are empirically known. By using the empirical models, ionospheric effects on radio propagation and GPS signal can be estimated to some extent. However, if the ionospheric density suddenly increases or decreases, the

empirical models cannot be applied to such phenomena, resulting in degradation of the radio signal. Such phenomenon is called an ionospheric storm. The ionospheric storm has a variety of scale sizes; a global-scale storm affects the whole Earth, and a small-scale storm affects only a specific region. It is important to understand various phenomena in the ionosphere for space utilization. The effects of magnetic storm on the ionosphere are complex and deviate greatly from average behaviour. There are some common elements of behaviour for most storms, but it has been recognized that in the low latitude regions the ionospheric response to particular geomagnetic storms manifests some irregularities (Rishbeth and Garriott, 1996).

2.4.4 Solar Wind Variations and Geomagnetic Storms

Geomagnetic disturbances are driven by solar wind-magnetosphere couplings. Solar wind energy is injected into the magnetosphere through field line merging of the inter- planetary magnetic field (IMF) and geomagnetic field. This energy injection is most efficient during southward IMF (Bs component). Prolonged periods of strong southward IMF will trigger geomagnetic storms. Observations have shown that a state of Bs > 10 nT lasting for over 3 hours will always generate a geomagnetic storm. Solar wind velocity (V) is another important factor. Geomagnetic storm development is known to demonstrate a strong positive correlation with the product of these two physical quantities, VBs. Two types of solar surface phenomena are believed to generate high VBs conditions: coronal mass ejection (CME) and coronal holes. CMEs are a phenomenon in which large amounts of solar coronal plasma is released into interplanetary space. CMEs appear simply as a region of high plasma density, but may contain a magnetic flux rope structure. The magnetic flux rope has a stable magnetic field structure. When the structure contains a stable southward magnetic field component, it is a significant driver of geomagnetic storms (Sahai et al., 2003).

2.4.5 Magnetic Indices

In the absence of direct measures of activity in the ionosphere and magnetosphere, the geomagnetic indices are used as proxies for the solar and geomagnetic disturbance levels. In turn, the majority of computational space weather simulations (empirical and physics based models) use geomagnetic indices to indicate the solar and geomagnetic disturbance levels. These magnetic indices were primarily intended to define discrepancies in the geomagnetic field, triggered by irregular current systems between the magnetosphere and ionosphere. Commonly these indices are derived from parameters which are monitored continuously with ground-based equipment. The space weather scientific community mostly makes use of the Kp, Ap and Dst indices, and Dst indices which are brief described chapter three. The

geomagnetic storms can be classified according to different Dst index levels as: weak level, moderate level, intense level, Super level and as shown below table. The Dst index values shows in Table 2.1.

Dst Index	Storm Type
-50 nT < Dst < -30 nT	Weak
-100 nT < Dst < -50 nT	Moderate
-200 nT < Dst < -100 nT	Intense
Dst < -200 nT	Super

Table 2. 1: The Dst index data were obtained from the World Data Centre for Geomagnetism, Kyoto (http://wdc.kugi.kyoto-u.ac.jp/index.html).

No	IGS station	Countries	Latitude	Longitude
1	BZRG	Italy	46.4988889	11.3366667
2	CAGS	Canada	45.5850000	-75.8072222
3	ESCU	Canada	47.0733333	-64.7986111
4	GRAZ	Austria	47.0669444	15.4933333
5	GANP	Slovakia	49.0344444	20.3227778
6	ZIMM	Switzerland	46.8769444	7.4650000
7	MIKL	Ukraine	46.9727778	31.9727778

Table 2. 2: shows the countries which IGS station found including their latitude and longitude.

Use of the Dst as an index of storm strength is possible because the strength of the surface magnetic field at low latitudes is inversely proportional to the energy content of the ring current, which increases during geomagnetic storms. In the case of a classic magnetic storm, the Dst shows a sudden rise, corresponding to the storm sudden commencement, and then decreases sharply as the ring current intensifies. Once the IMF turns northward again and the ring current begins to recover, the Dst begins a slow rise back to its quiet time level(see figure 2.9,&2.10,2.11).

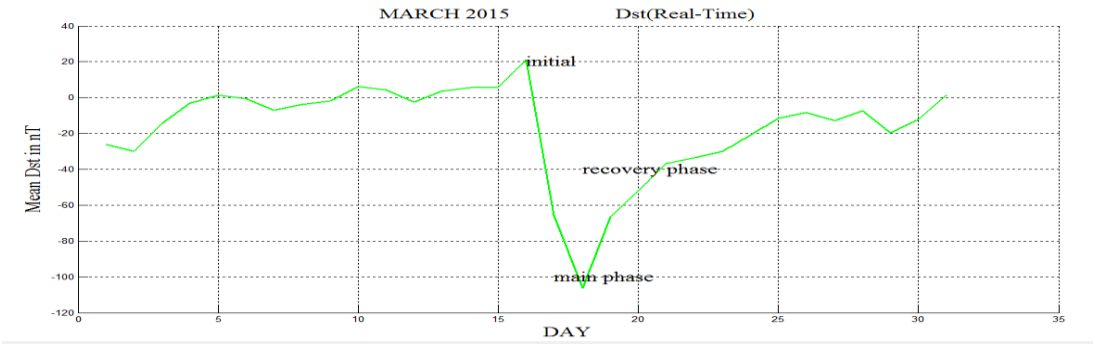

Figure 2. 9: Time (day) vs Dst index values for March 2015.

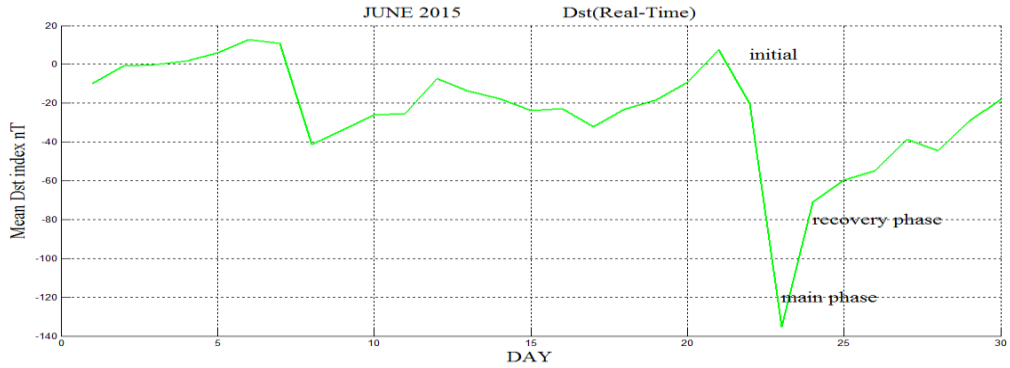

Figure 2. 10 : Time (day) vs Dst index values for JUNE 2015.

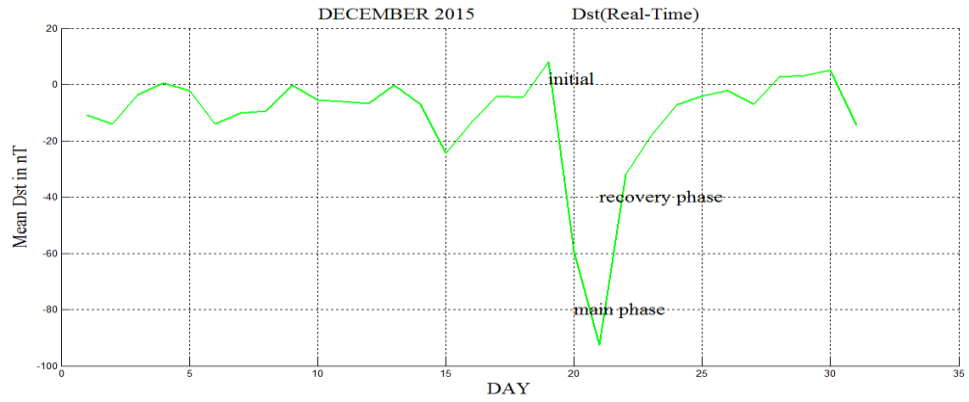

Figure 2. 11: Time (day) vs Dst index values for December 2015.

Storm day	Storm level
March 17	224nT(intense)
June 23	215nT (intense)
December 20	155 nT (moderate)

Table 2. 3 storm day with storm level.

Chapter Three

3. Material and Methodology

3.1 Data Source

In this study, we used GPS data (TEC) for the geomagnetic storm that take place in March 16, 17 &18, June 22, 23, 24 and December 19, 20&21 year 2015 from selected IGE station list are distributed in during North America (Canada), Europe (Italy, Ukraine, Switzerland, Switzerland, Slovakia and Austria) in selected IGS station. Geomagnetic activities are measured by Dst index.TEC data are used to study the ionospheric scintillation, and rate of change of total electron content index. The Material was used to studied this study using UNAVCO down load software, GGrun 2016 ,and matlab.The geomagnetic storm data was taken from Kyoto University.The TEC data are downloaded from UNAVCO data home page http://facility.unavco.org/data/gnss/perm-sta.php.The observed changes in geomagnetic field during geomagnetic storm are essentially a consequence of strong and rapid magnetospheric processes and changes under solar wind action. The raw data was processed using software. The Dst or disturbance storm time index is a measure of geomagnetic activity used to assess the severity of magnetic storms. It is expressed in nanoteslas and is based on the average value of the horizontal component of the Earth's magnetic field measured hourly at four near-equatorial geomagnetic observatories.

Use of the Dst as an index of storm strength is possible because the strength of the surface magnetic field at low latitudes is inversely proportional to the energy content of the ring current, which increases during geomagnetic storms. In the case of a classic magnetic storm, the Dst shows a sudden rise, corresponding to the storm sudden commencement, and then decreases sharply as the ring current intensifies. Once the IMF turns northward again and the ring current begins to recover, the Dst begins a slow rise back to its quiet time level(see figure 2.9,2.10&2.11).

3.2 Data Analysis

3.2.1 Ionospheric Total Electron Content (TEC)

In the recent years, the measurements of total electron content (TEC) have initiated great interest due to highly increasing demands in the GPS-based technologies, navigation

applications, in trans-ionospheric communications with space-borne vehicles, such as satellites, aircrafts and surface transportations. The TEC measurements are obligatory in order to make an appropriate range delay correction which is happened by the ionosphere, both during quiet (periods without ionospheric disturbance) and disturbed periods (space weather events). TEC is one of the most important quantitative parameters of the Earth's ionosphere and plasma sphere.

Total Electron Content (TEC) is defined as the total number of electrons integrated along the path from the receiver to each GPS. TEC is an indicator of ionospheric variability that is derived by the modified GPS signal through free electrons.

Mathematical expression for the computations of TEC in the slant direction given by equation 3.1.

$$STEC = \int_{R}^{S} N_e(\lambda, \varphi, h)\, ds \ldots\ldots\ldots\ldots\ldots\ldots\ldots\ldots\ldots\ldots\ldots\ldots\ldots\ldots\ldots (3.1)$$

where R stands for receiver, S stands for satellite, ds stands for infinitesmal distance is $N_e(\lambda, \varphi, h)$ as the ionospheric electron density, and λ, φ and h are the longitude, latitude and height, respectively.

If one knows the electron density at a height h latitude φ and at a longitude λ one can determine the total electron content all the way from the receiver to the satellite (Ubaidi and Ali, 2013) see figure 3.4.

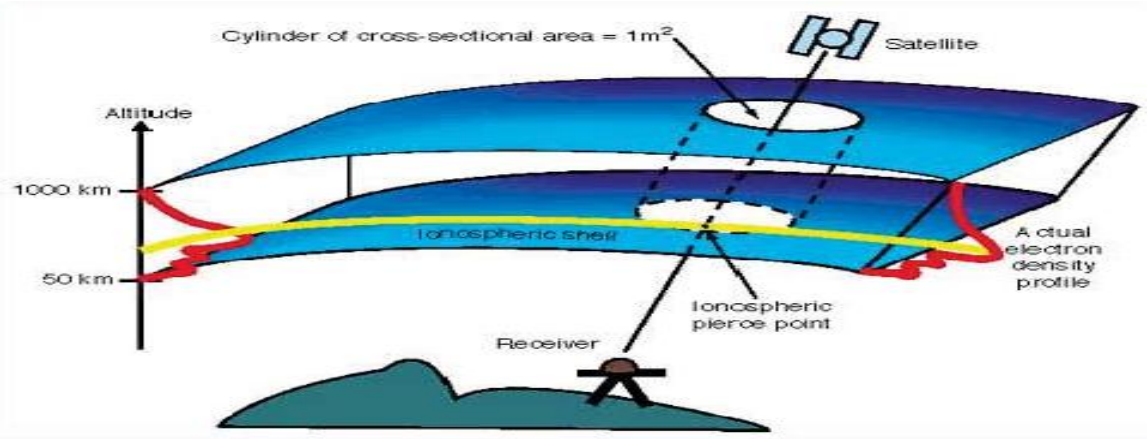

Figure 3. 1: A total electron content through 1 m^2 area cylindrical tube (from http //docslide:us/documents/atmosphere.

The rate of the TEC index (ROTI, in TECU/min) can be used to describe the measurements of ionospheric irregularity and scintillation activity. The rate of TEC (ROT, in TECU/min) is measured by utilizing dual-frequency GPS observation phase data, and computing the relative TEC changes, epoch by epoch, along the signal paths from each individual to the receiver, as

shown in Equation (3.2). The index ROTI is defined as the standard deviation of ROT over a 5-min time interval, as shown in Equation (3.2).

$$ROT = \frac{\Delta STEC}{\Delta t} \ldots\ldots\ldots\ldots\ldots\ldots\ldots\ldots\ldots\ldots\ldots\ldots (3.2)$$

$$ROTI = \sqrt{\langle ROT^2 \rangle - \langle ROT \rangle^2}. \ldots\ldots\ldots\ldots\ldots\ldots\ldots (3.3)$$

where STEC represents the TEC along the ray path from the satellite to the receiver (in TECU) and Δt (in seconds) denotes the sampling interval.

Use ROTI to determine presence of amplitude and phase scintillation (Mannucci et al, 1997).

(Mannucci et al, 1997) used ROTI to determine the occurance of amplitude and phase scintillation .This study aims to incorporate the effect of ROTI on phase scintillaton.

Chapter Four

4. Result and Discussion

4.1 Introduction

In this section, we analyse and discuss the characteristics of VTEC, ROT and ROTI fluctuations over Canada and Europe using selected IGS station during geomagnetic storm. The elevation angle is 25 degree and the average latitude value is 47 degree. Magnetic storm is a global event characterized by disturbances of the Earth's magnetic field. It includes three phases: initial phase, main phase and recovery phase. These phases are identified in observations from low latitude magnetometers reflecting changes in the large-scale near-earth ring current (Mannucci et at, 1997). Ionospheric storm was occurred in 2015 in three months; March, June and December. Ionospheric effects are typically characterized by measuring their impact on the amplitude and phase of the received GNSS signal. The most commonly used measures are the scintillation indices (i.e., amplitude and phase) and the ROT rapid changes (rate of TEC). It is evident that during a storm, the intensity of ROT fluctuations is essentially increased. The irregularity oval expands towards equator with increased magnetic activity. The occurrence of irregularities is strongly dependent on geomagnetic activity. Therefore, using the GPS network and the GPS phase fluctuation index ROTI, it is possible to monitor global activity of the ionospheric irregularities (Ubaidi and Ali, 2013).

4.2 Longitudinal dependency of Ionospheric Scintillation during Geomagnetic Storm

To explain ionospheric scintillation behaves longitudinally during geomagnetic storm by the Variations of VTEC, ROT and ROTI. The cause of the storm is dramatic responses in the ionospheric- plasma sphere- magnetosphere system. The universal time dependency of the east-west difference in TEC is a significant characteristic.

4.2.1 Variations of VTEC, ROT and ROTI during Geomagnetic storm in March (16, 17 and 18), 2015

The vertical total electron content (VETC) variation on March (16, 17 and 18) of the year 2015 was depicted in figure 4.1 .The blue colour shows that the longitudinal variations of vertical total electron content (VTEC) on March 16, 2015. VTEC across BZRG, GANP, ZIMM and GRAZ (0-5) stations as constancy from (5-10) hour is increased, 10-12 hour

slightly decreased and (12-24) hour is decreased. Whereas VTEC across CAGS and ESCU has decreased from 0-4hours remined constant between, 4-11 hours, later increased from 11-15hour and even finally remind constant between 16-24hour. VTEC from in MIKL 0-4hour became constant, 4-6hour constant, 6-11hour is increased and 11-24 decreased. The magenta colour shows that the longitudinal variations of vertical total electron content (VECT) on the 17th March, 2015.

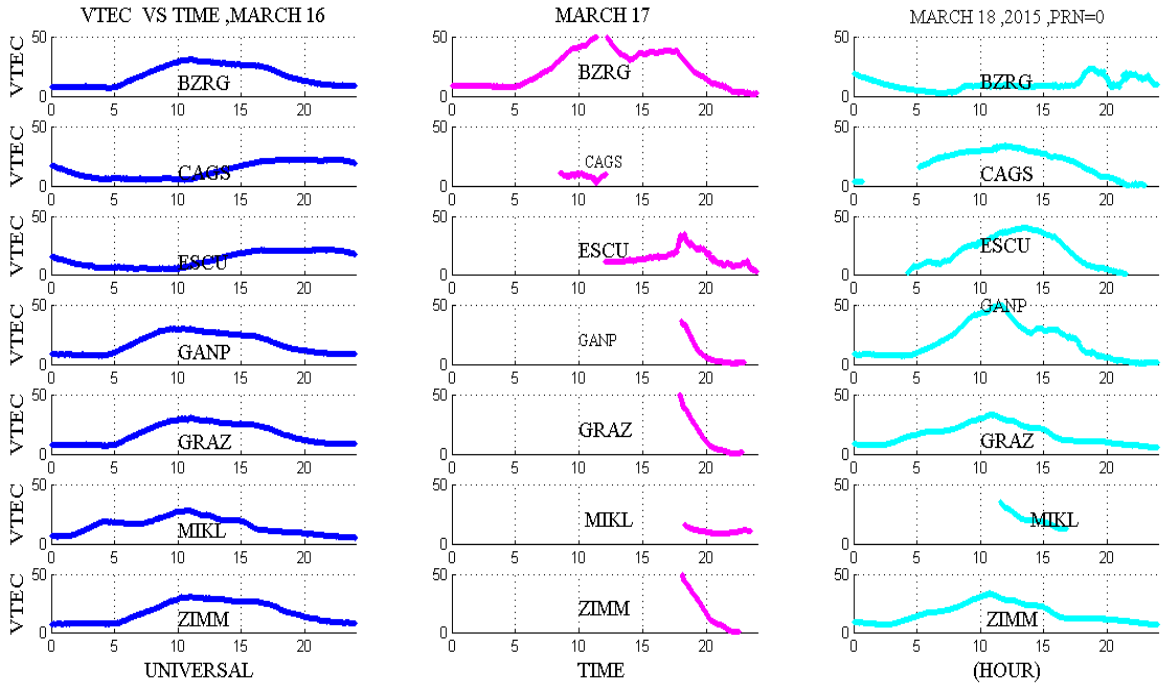

Figure 4. 1: The variations of VTEC (at PRN = 0) for IGS station (BZRG, CAGS, ESCU, GANP, GRAZ MIKL and ZIMM) sites in March (dyas16, 17, and 18).

In figure 4.1The vertical axis is of the VTEC value and the horizontal axis represents time in hours. The PRN numbers of each subfigure is 0. The blue colour shows initial phase, magenta colures are the recovery phase and the green colour is recovery phase.

VTEC in BZRG 0-5hour is constant, 5-10hour is increased, 11-14hour decreased, 14 -17hour is increased, 17 -21hour is decreased and 21-24hour constant and it is observed. VTEC in CAGS 8- 12hour is constant and the remaining hour there is no data. VTEC in ESCU 12-18hour is constant, 18-19hour is increased and finally 19-24hour is constant. VTEC in GANP, GRAZ, KILM and ZIMM from 18-24hour is decreased and the variation is observed. The green colour shows that the longitudinal variations of vertical total electron content (VECT) on March 18, 2015. The cause of variations is the occurrence of geomagnetic storm. VTEC in BZRG, 0-6hour is decreased,6-9hour is increased,9-16hour is constant,16-17hour is increased,17-20hour is decreased,20-21hour is increased and 21-24hour is decreased. VTEC

in CAGS, 0-5hour there is no data, 5-11hour is increased and 11-24hour is decreased. VTEC in ESCU, 0-5hour has no data,5-12hour and half hour is increased, 12 and half-22hour is decreased. VTEC in GANP, 0-5hour is constant, 5-10hour is increased, 10-20hour is decreased and finally 20-24hour constant. VTEC in GRAZ, 0-11hour is increased and 11-24hour is decreased. VTEC in MIKL around 12-17hour is decreased and the remaining is not observed. VTEC in ZIMM, from 0-11hour is increased and 11-24hour is decreased.

The ROT variation on March (16, 17 and 18) 2015 depicted below Figure4.2. The blue colour shows that the longitudinal variations of ROT on March 16, 2015. The variations of ROT in BZRG, from 0-24hours is fluctuated and ionospheric scintillation is observed, in CAGS 0-24hour is fluctuated and high fluctuation is observed from five up to seven hours, in ESCU from 0-4hour and 11-24 hour the fluctuation is slow and from 4-11hour is fluctuated is high, in GANP, GRAZ, MIKL and ZIMM from 0-24hour is fluctuated and GRAZ from nine up to eleven hours is highly fluctuated.

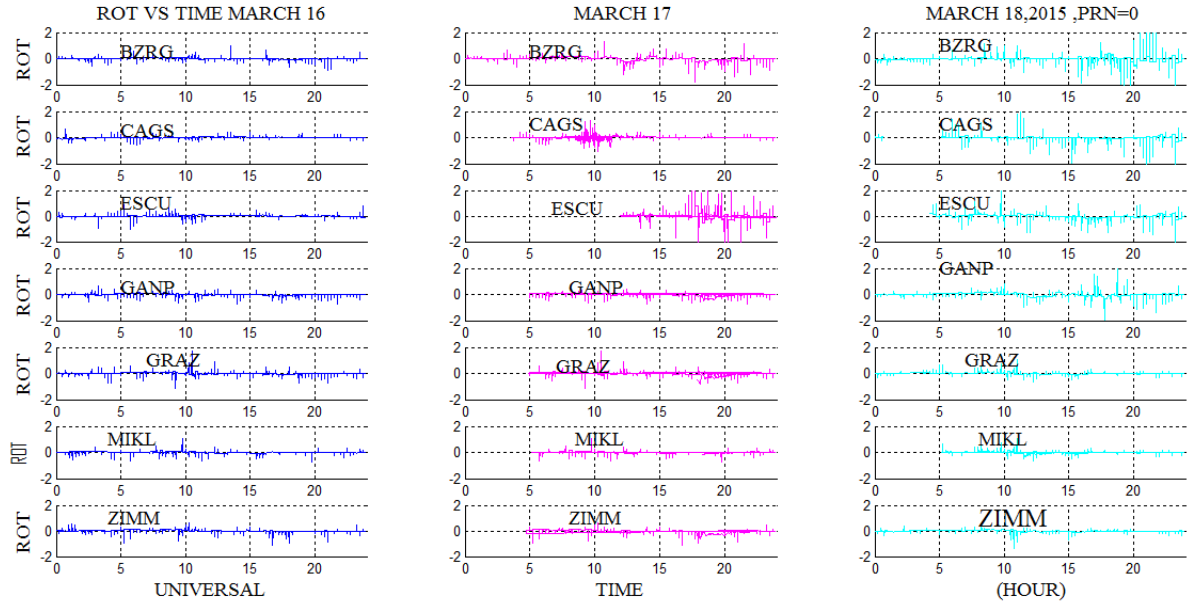

Figure 4. 2*: The variations of ROT (at PRN = 0) for IGS station (BZRG, CAGS, ESCU, GANP, GRAZ MIKL and ZIMM) site (March 16, 17 and 18).*

The vertical axis is of the ROT value and the horizontal axis time in hours. The PRN numbers of each subfigure is 0. The blue colour shows that the initial phase, magenta colures are the recovery phase and the green colour is recovery phase. The magenta colour shows that the longitudinal variations of ROT on March 17, 2015.In this day maximum variations observed (ESCU), while the minimum variations (MIKL). The variations of ROT in BZRG 0-24 hour is fluctuated, in CAGS 0-4hour has no data,4-11huor is high fluctuated and the remaining

hour the fluctuation is minimum, in ESCU 0-13hour has no data,13-24hour is highly fluctuated, in GANP, GRAZ, MIKL & ZIMM from 0-5hour has no data and 5-24hour is fluctuated. The green colour shows that the longitudinal variations of ROT on March 18, 2015.In this maximum variation (BZRG), while the minimum variations (ZIMM) observed. The cause of variations is the occurrence of geomagnetic storm. The variations of ROT in BZRG from 0-8hour the fluctuation is small & from8-15hour the fluctuation is medium and 15 -24hour fluctuation is high, in CAGS and ESCU from 0-5hours has no data and 5-24hours is fluctuated, In GANP from 0-9hours the fluctuations are small 9-16hour fluctuation is medium and from 16-24hour the fluctuation is high and GRAZ and in MIZZ 0-24hours is fluctuated but the fluctuation is small. The ROTI variation in March (16, 17 and 18) of the year 2015 was show bel figure 4.3. The blue colour shows the longitudinal variations of ROTI on March 16, of the year 2015.

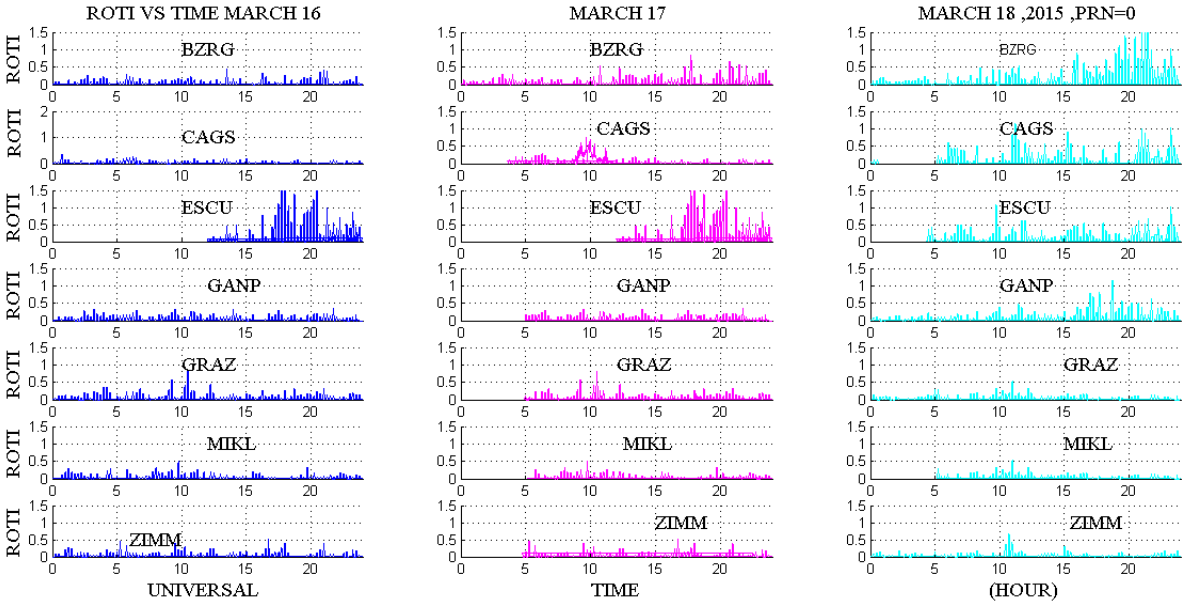

Figure 4. 3*: The variations of ROTI (at PRN = 0) for all of the observed GPS satellites at the BZRG, CAGS, ESCU, GANP, GRAZ MIKL and ZIMM site on (March 16, 17 and 18).*

In the figure 4.2The vertical axis is of the VTEC value and PRN number of the corresponding satellite. The PRN numbers of each subfigure is 0. The blue colour shows initial phase, red colures are the recovery phase and the green colour is recovery phase.

Typically, TEC fluctuations satisfying ROTI ≥0.5 indicate the occurrence of irregular ionospheric activities relevant to ionospheric scintillation (Yang, Z. and Liu, Z., 2015). In this study, we wanted to conduct a more in-depth quantitative analysis of the intensity of ionospheric disturbances and their occurrence ratio over Canada (CAGS and ESCU) and Europe (Italy, Switzerland, Ukraine, Slovakian and Austria. As such, we based our analysis

on the original ROTI value, which requires that the standard level of TEC fluctuations be preliminarily divided into three groups: weak if 0.25≤ROTI<0.5; moderate if 0.5≤ ROTI <1; and strong if ROTI ≥1. The daily occurrence ratio is the ratio of the TEC fluctuation epoch numbers to all of the observed epoch numbers with in one day (Ubaidi and Ali, 2013).

The blue colour shows that the longitudinal variations of ROTI on March 16, 2015. ROTI fluctuation and variation in the seven IGS station show as following. In BZRG, CAGS, GANP, GARZ, MIKL and ZIMM the fluctuation is small or weak or the TOTI value is small for 0-24hour. In ESCU 0-11hour has no data and 11-24hour the value of ROTI is maximum or strong. The magenta colour shows that the longitudinal variations of ROTI on March 17, 2015. In BZRG from 0-8hour the value of ROTI is small, 8-16hour ROTI value is medium and 16-24hours the value of ROTI very high. In CAGS, ESCU and MIKL from 0-5hour has no data and 5-24hour ROTI value is high but in MIKL it is small. In GANP and GRAZ from 0-11hour the value of ROTI is very small and in GANP from 11-16hour its ROTI value is medium and 16-24hour is high. While in GRAZ from 11-24hour ROTI is minimums. The green colour shows that the longitudinal variations of ROTI on March 18, 2015.In this maximum variation (BZRG), while the minimum variations (ZIMM) observed. The cause of variations is the occurrence of geomagnetic storm.

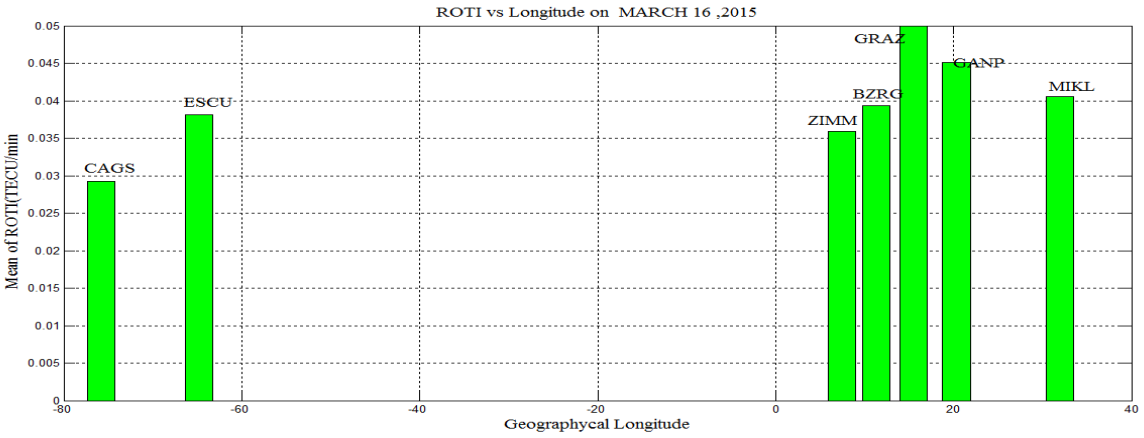

(a)

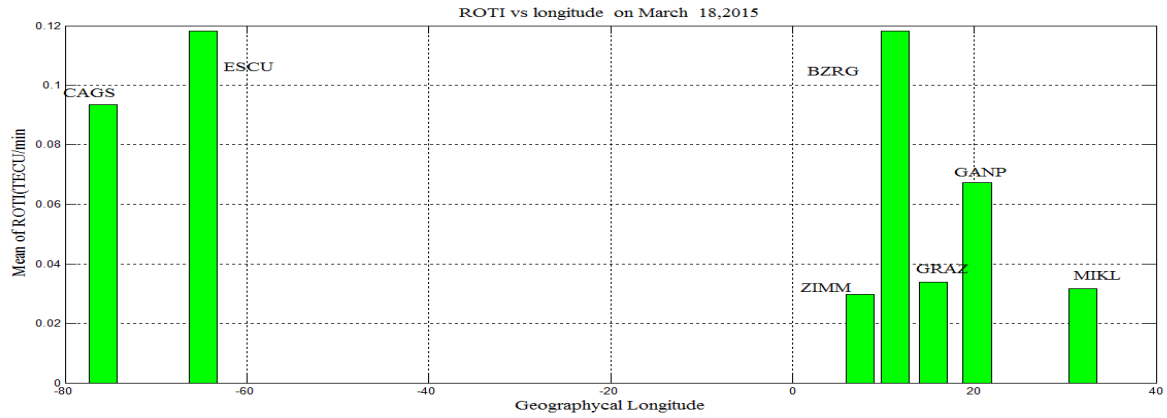

(b)

Figure 4. 4: Geographical Longitude vs the mean of rate of TEC Index (ROTI) of the seven station at PRN = 0 on March 16 &18, 2015.

1n figure 4.4The horizontal axis denotes geographical longitude and the vertical axis represents ROTI. As depicted from the figure 4.4 (a), low value of ROTI is observed in Canada (CAGS) and highest of in Austria (GRAZ). Figure 4..4 (b) show low value of ROTI is observed in Canada (CAGS) and high value in Canada (ESCU) and Italy (BZRG).

4.2.2 Variations of VECT, ROT and ROTI during geomagnetic storm on June 22, 23 and 24, 2015

The vertical total electron content (VTEC) variation that takes places in June 22, 23 & 24 in the year ass 2015 depicted on figure 4.5. The blue colour shows was the longitudinal variations of vertical total electron content (VECT) in June 22, 2015 maximum variation in VTEC occurred 10 hours (BZRG, ZIMM and MIKL) and at 9 -11 hours (GANP) observed, while the minimum variations at 10 hours (CAGS and ESCU). The variations of VTEC in BZRG 0-11hour are increased, 11-12hour is decreased, and 12-16hour is constant, 16-18hour increased and 18-24hour decree-sed. In CAGS 0-9 hour decreased, 9-19hour increased, 19-21hour is constant and 21-24hour is increased. In ESCU 0-9hour is decreased, 9-19hour is increased 19-24 decreased. The magenta colour shows the longitudinal variations of vertical total electron content (VECT) on June 23, 2015.In this day maximum variations is observed at 11 hour (GANP). The variations of VTEC in BZRG 0-1hour increased, 1-10 hour and 15-24 hour constant, in CAGS 0-10hour decreased and 10-24hour is increased. In ESCU 0-6hour is decreased, 6-8hour constant,8-24hour is increased. In GANP 0-5hour is constant, 5-11hour

is increased and 11-24hour is decreased. In GRAZ, ZIMM and ZIMM 0-10hour is constant and from 10-24hour is slightly decreased.

The green colour shows that the longitudinal variations of vertical total electron content (VECT) on June24, 2015.In this maximum variation hours (GANP) is observed, while the minimum variations at CAGS and ESCU.The cause of variations is the occurrence of geomagnetic storm. The variations of in BZRG 0-10hour and 16-24hour is constant, in CAGS and ESCU 0-5hour is decreased, 5-8hour is constant and 8-24hour is increased. In GANP, GRAZ and ZIMM 0-4hour is consant.4-11hour is increased and 11-24hour.

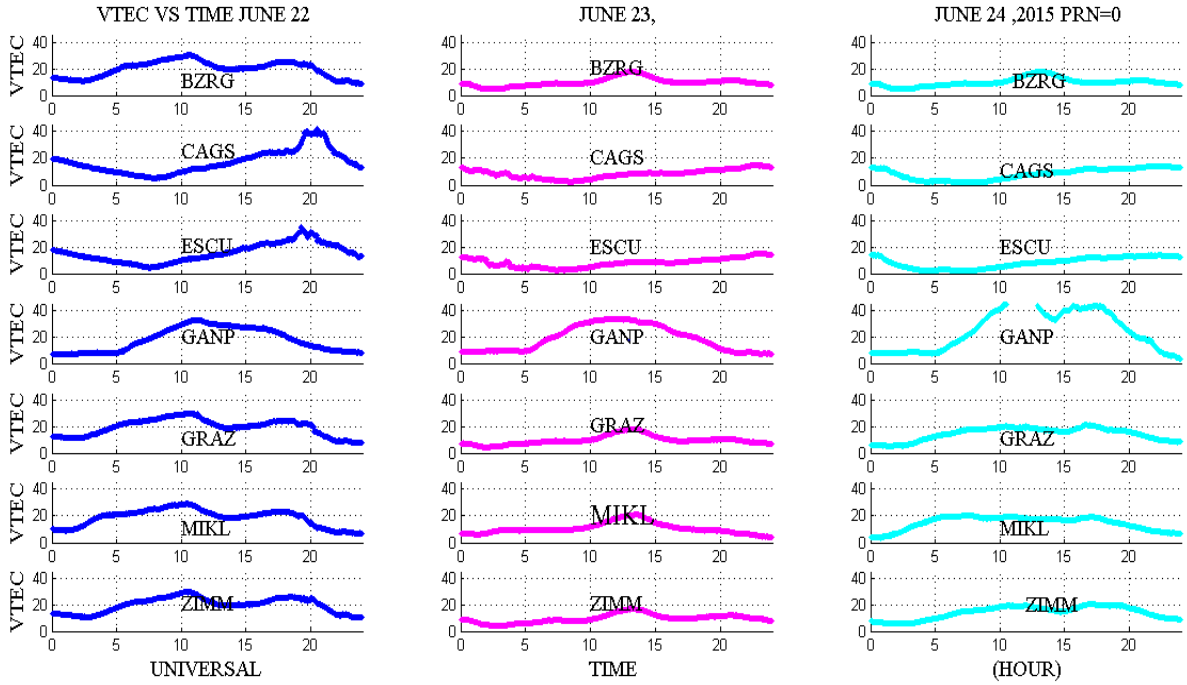

Figure 4. 5:*The variations of VTEC for all of the observed GPS satellites at the BZRG, CAGS, ESCU, GANP, GRAZ MIKL and ZIMM site June 22,23 & 24 in 2015.*

In figure 4.5the vertical axis represents VTEC value and the horizontal axis denotes time in hour. The PRN numbers of each subfigure is 0. The blue colour shows initial phase, magenta colour is the main phase and the green colour is recovery phase.

The variation Rate of total electron content (ROT) in June 22, 23 & 24 in 2015 as shown in figure 4.6. The blue colour shows longitudinal variations of vertical total electron content (ROT) on June 22, 2015. The cause of variations is the occurrence of geomagnetic storm. In BZRG, GANP, GRAZ MIKL and ZIMM, is observed fluctuation from 0-24hour but the fluctuation is small. In CAGS&ESCU from 0-16hour the fluctuation is minimum, and 16-24 is maximum fluctuated. The magenta colour shows that the longitudinal variations of vertical total electron content (ROT) on June 23, 2015. In BZRG, GANP, MIKL and ZIMM 0-24hour

is fluctuated, but the fluctuation is small. In CAGS and ESCU which is from 0-6hour is fluctuated and from 6-24hour fluctuated is minimum. The green colour shows the longitudinal variations of Rate of total electron content (ROT) on June 24, 2015. In BZRG, CAGS, ESCU MIKL GRAZ and ZIMM 0-24hour is fluctuated but the fluctuation is small, and in GANP 0-10hour is observed small fluctuation and 10-24hour observed high fluctuation .The cause of variations is the occurrence of geomagnetic storm.

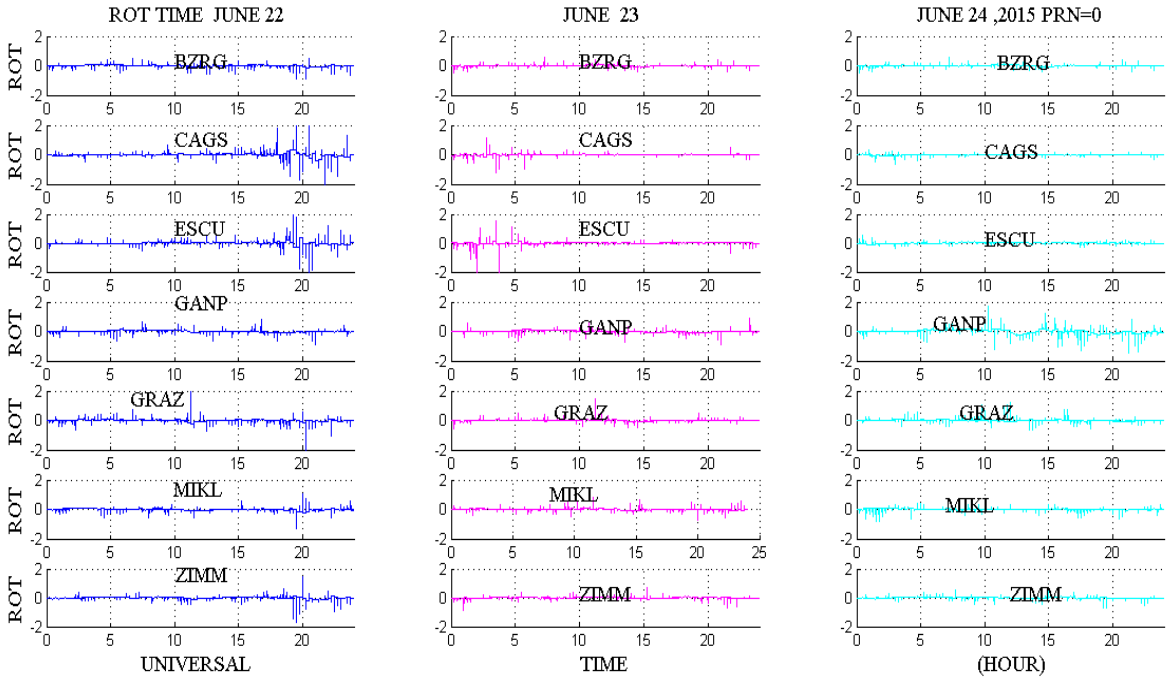

Figure 4. 6*: The variations of ROT (at PRN = 0) for IGS station (BZRG, CAGS, ESCU, GANP, GRAZ MIKL and ZIMM) site on June (days 22, 23, and 24).*

In the figure 4.6 vertical axis denotes ROT value and the horizontal axis represents time in hours. The PRN numbers of each subfigure is 0. The blue colour shows initial phase, magenta colour as the recovery phase and the green colour is recovery phase.

The variation Rate of total electron content index (ROTI) on June 22, 23 & 24 in 2015 depicted below Figure 4. 7. The blue colour shows the longitudinal variations of Rate of total electron content index (ROTI) on June 22, 2015.The variations of ROTI in all IGS station from 0-24hour observed fluctuation but the maximum fluctuation is observed from 18-24hour in Canada (CAGS, and ESCU). The magenta colour shows longitudinal variations of Rate of total electron content index (ROTI) on June 23, 2015. The variations of ROTI in all IGS station from 0-24hour observed fluctuation but the maximum fluctuation is observed from 0-5hour in Canada (CAGS and ESCU). The green colour shows the longitudinal variations of

Rate of total electron content index (ROTI) on June 24, 2015. The variations of ROTI in all IGS station 0-24hours is fluctuated, the maximum variation is observed in GANP from 10-24hour and GRAZ from 9-12hour.

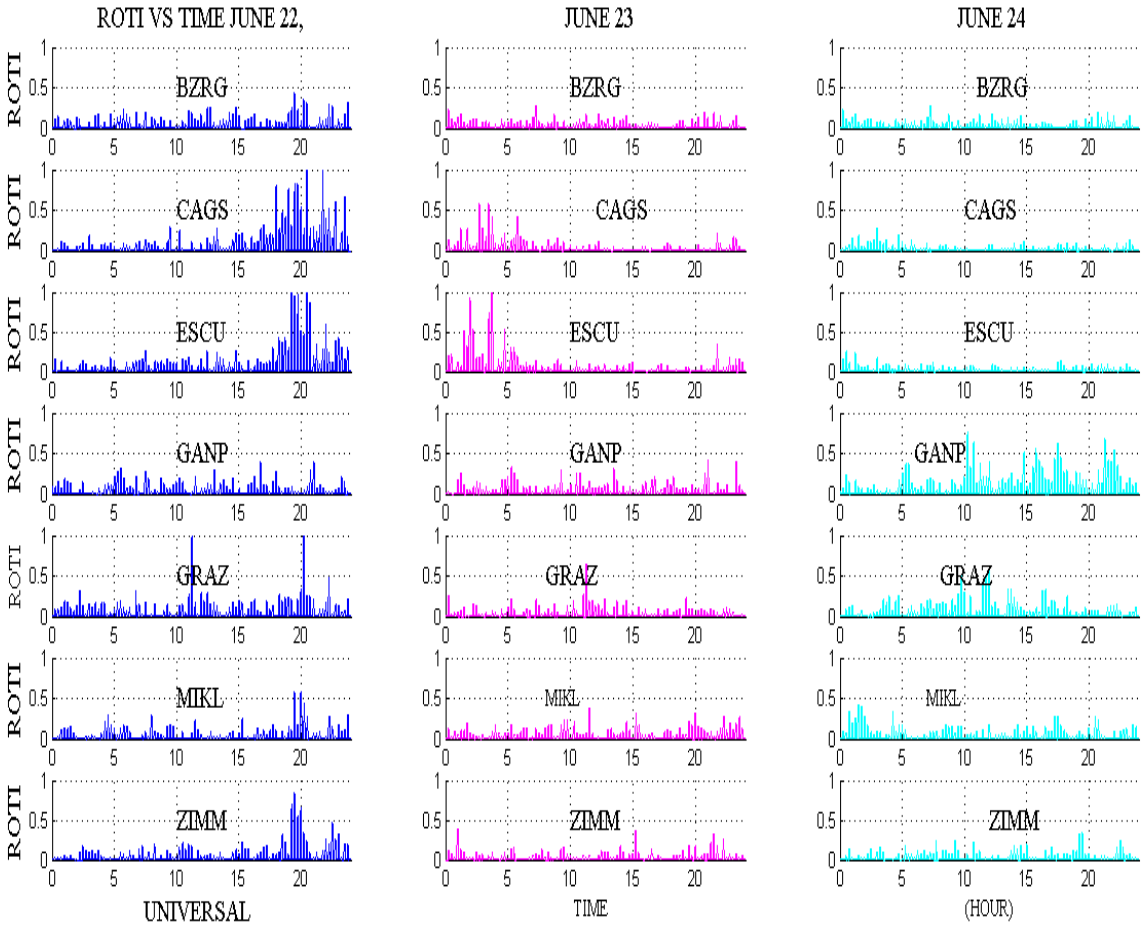

Figure 4. 7 :The variations of ROTI (at PRN = 0) for IGS station (BZRG, CAGS, ESCU, GANP, GRAZ MIKL and ZIMM) site June (days 22, 23, and 24).

The vertical axis is of the ROTI value and the horizontal axis as time in hours. The PRN numbers of each subfigure is 0. The blue colour shows initial phase, in magenta colour as the recovery phase and the green colour is recovery phase.

The blue colour shows that the longitudinal variations of Rate of total electron content (ROT) on June 22, 2015.The variations of ROTI in BZRG and GANP 0-24hour fluctuated. In CAGS, ESCU, MIKL and ZIMM 0-19hour is fluctuated and 19-24hour is fluctuated. In GRAZ 11&20hour is fluctuated, and the rest hours no fluctuation. The magenta colour shows the longitudinal variations of Rate of total electron content (ROT) on June 23, 2015. The variations of ROTI in BZRG, GANP, and MIKL &ZIMM 0-24hour are fluctuated. In CAGS and ESCU 0-5hour are fluctuated and 5-24hour no fluctuation. In GRAZ 0-24hour is slowly

fluctuated. The green colour shows that the longitudinal variations of Rate of total electron content (ROT) on June 24, 2015.

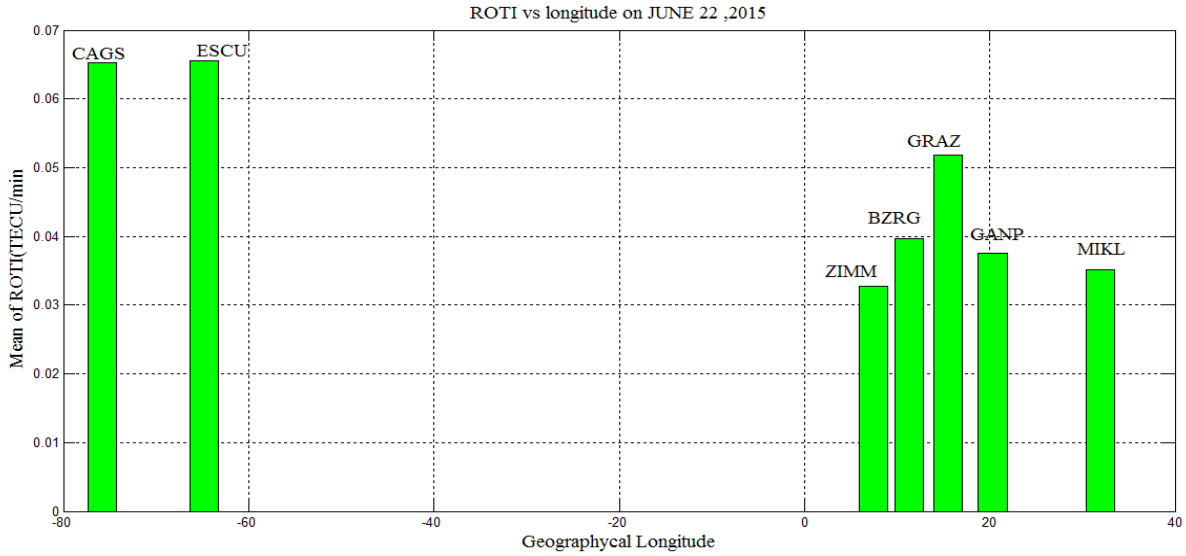

(a)

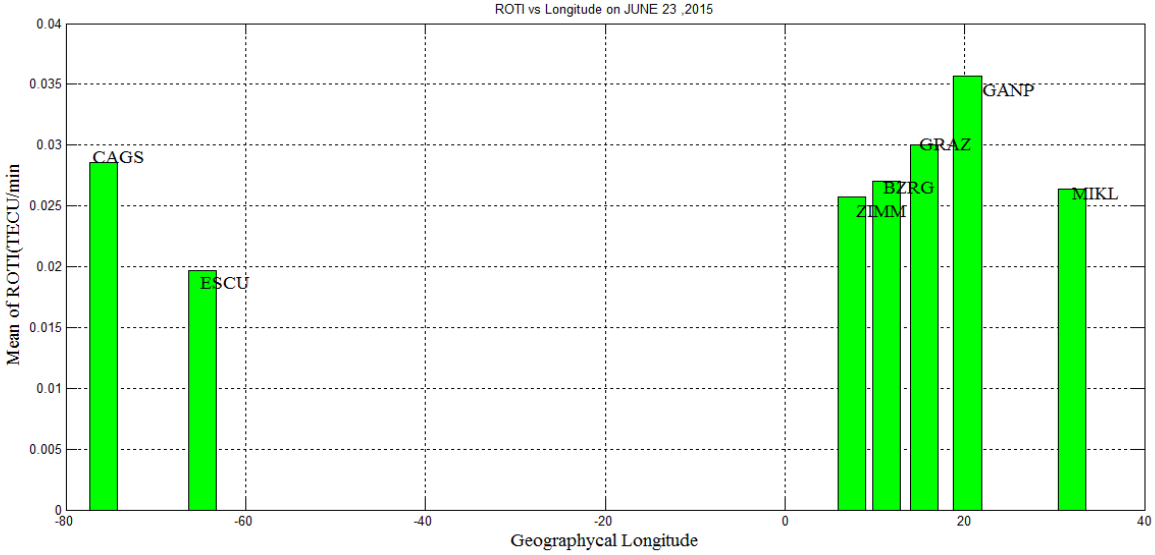

(b)

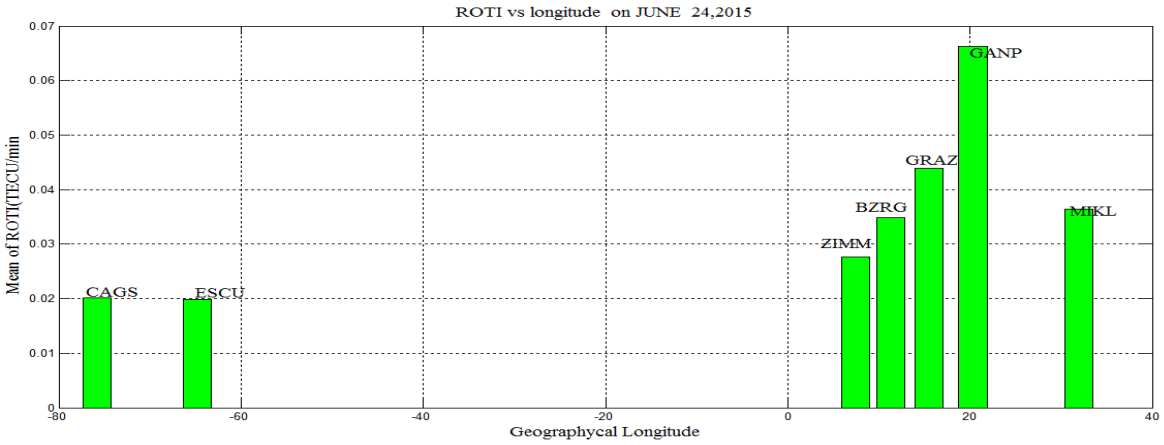

©

Figure 4. 8 : The mean of Rate of TEC Index (ROTI) vs Geographical Longitude of the seven stations at PRN=0 in June 22-24, 2015.

In the figure 4.8 the horizontal axis is geographical longitude and the vertical axis is ROTI. This graph is shows longitudinal variations of phase scintillation during geomagnetic storm. In the figure 4.8 shown above (a), maximum value of ROTI is observed in Canada (ESCU&CGAS) and the minimum value is of ROTI Switzerland (ZIMM); (b), maximum value of ROTI is observed in Slovakia and the minimum value is of ROTI Canada (ESCU) (c) maximum value of ROTI is observed in Slovakia (GANP) and the minimum value is of ROTI is Canada (CAGS & ESCU).

4.2.3 Variations of VECT, ROT and ROTI during geomagnetic storm on December (days:19, 20 and 21, 2015

The vertical total electron content (VECT) variation in December 0n19, 20 & 21 in 2015 is depicted in Figure 4. 9. The blue color shows that the longitudinal variations of vertical total electron content (VECT) on December 19, 2015. The variations of VECT in BZRG, GRAZ and ZIMM from, 0-6&16-24hour is constant and 6-11 hour is increased, in CAGS and ESCU, 0-11hour is constant, 11-18hour is increased, 18-24hour. In GANP 0-5hour is has no data, 5-12hour is increased, and 12-24hour is increased. The magenta colour shows that the longitudinal variations of vertical total electron content (VECT) on December 20, 2015. The variations of VECT in BZRG ,0-6hour constant,6-9hour is increased ,9-10hour is decre - ased,10-11hour increased,11-13hour is decreased,13-15hour is increased and 15-14hour is decreased. In CAGS 0-20hour is increased and 20-24hour is decreased. In ESCU 0-15 &16-24 hours have no data and 15-16hour slightly increased. In GARZ 0-6 hour has no data, 6-

14hour is increased and 14-24hour decreased. GRAZ 0-6hour is constant, 6-9hour is increased, 9-10hour is decreased, 10-12hour is increased and 12-24houris decreased. In MIKL 0-5hour is constant, 5-9hour is increased, 9-10hour is decreased, 10-11hour is constant and 11-24hour is decreased. In ZIMM 0-6hour is constant, 6-9hour is decreased, 9-10hour is increased, 10-13hour is decreased, 13-15hour is increased and 15-24hour is decreased. The green colour shows that the longitudinal variations of vertical total electron content (VECT) on December 21, 2015. The variations of VECT in BZRG, GRAZ and ZIMM from 0-6hour is constant 6-11hour is increased, 11-20hour is decreased, 20-24hour is constant. In CAGS and ESCU from 0-11hour is constant, 11-19hhour is increased, and 19-24hour is decreased. In GANP 0-1hour decreased, 1-6houris slightly increased 6-11hour is constant,11-13hours is increased,13-16houris decreased,16-21hour is constant and 21-24hour is decreased.

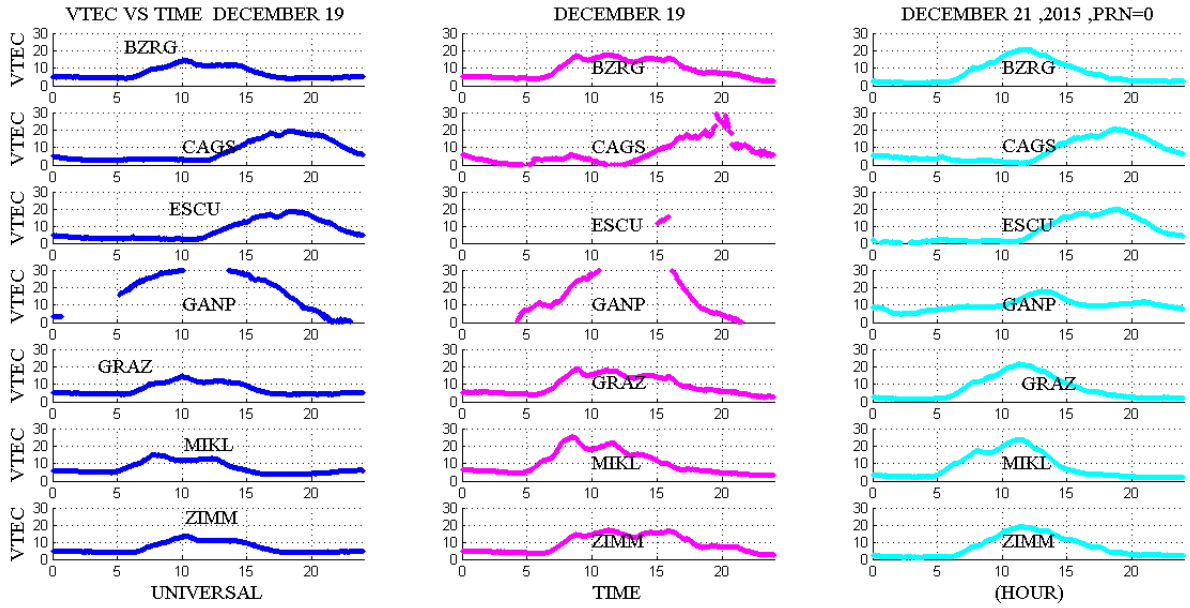

Figure 4. 9*: The variations of vertical electron content (VTEC) (at PRN = 0) for IGS station (BZRG, CAGS, ESCU, GANP, GRAZ MIKL and ZIMM) site (March 16, 17, and 18).*

In figure 4.9 the vertical axis represents of the VTEC value and the horizontal axis denotes time in hours. The PRN numbers of each subfigure is 0. The blue colour shows initial phase, magenta colour as the main phase and the green colour is recovery phase.

The variations of the rate of total electron content (ROT) is shows in figure 4. 10. The blue colour represents the initial phase on December 19, 2015. The variations of ROT in BZRG, CAGS, ESCU, GRAZ, MIKL and ZIMM are observed minimum fluctuation in 0- 24hours, and in GANP 0-5hour has no data and 5-24hour is observed high fluctuation. The magenta colours represent the main phase on December 20, 2015. The variations of ROT in BZRG, ESCU, GRAZ, MIKL and ZIMM are observed minimum fluctuation from 0- 24hours and in

GANP 0-5hour have no data and 5-24hour is observed fluctuation. In CAGS 0-16hour observed minimum fluctuation, and 16 -24 hour observed high fluctuation. The green colour represents the recovery phase on December 21, 2015. The variations of ROT in all station are observed minimum fluctuation for 0- 24hours.

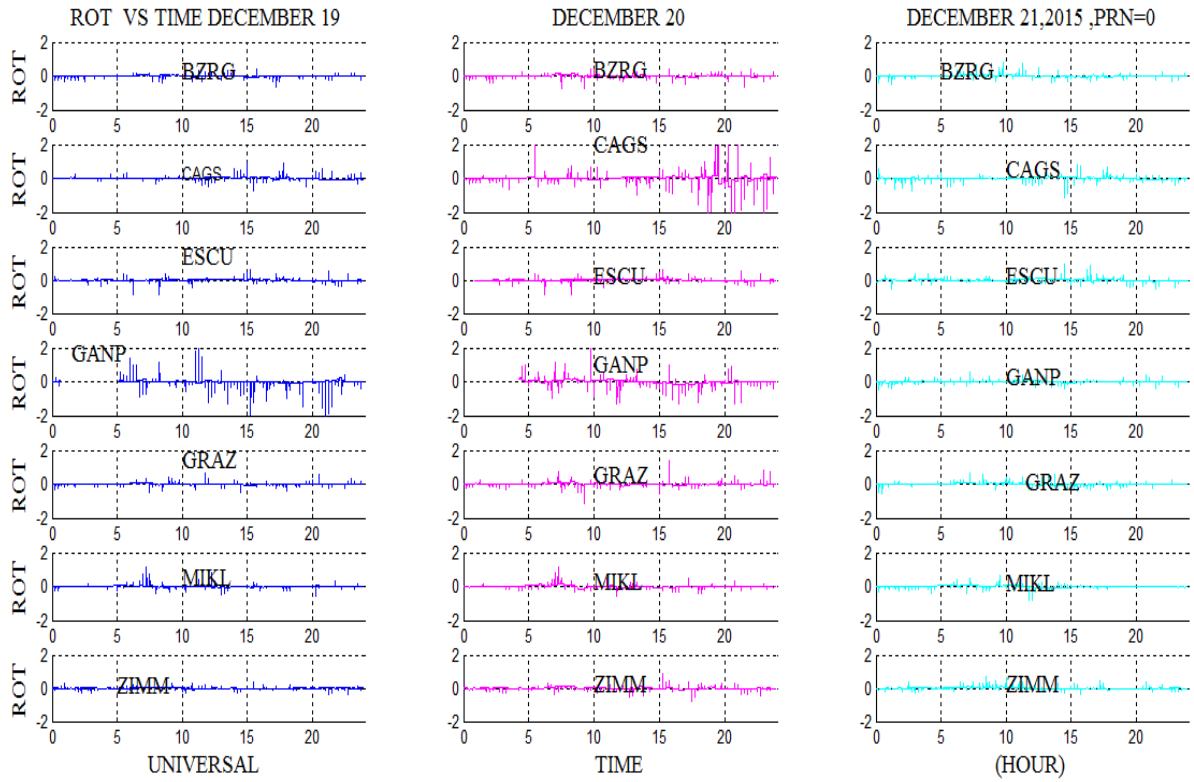

Figure 4. 10*: The variations of Rate of Total electron content (ROT) (at PRN = 0) for IGS station (BZRG, CAGS, ESCU, GANP, GRAZ MIKL and ZIMM) site (December 19, 20 and 21).*

In figure 4.10 the vertical axis represents of the ROT value and the horizontal axis denotes time in hours. The PRN numbers of each subfigure is 0. The blue colour shows initial phase, red colour as the main phase and the green colour is recovery phase.

Figure 4.11 show that the variations of rate of change of total electron content index (ROTI) in December (19,20and 21), 2015. The blue colour indicates the variation on VTEC on 19th December years 2015. The maximum fluctuation is observed in GANP from 5-24 hours, and from 0-5hours has no data. The remaking of the rest six IGS station is observed minimum fluctuation. He magenta colour is indicate that the variations of ROTI on December 20, 2015. In IGS station BZRG, ESCU, GRAZ, GANP, MIKL and ZIMM from 0-24houur is observed minimum fluctuation. In CAGS (Canada) from 0-16hour is observed minimum fluctuation and 16-24hour the fluctuation is maximum. In GANP from 0-5hour has no data or the

satellite is not recorded data, 5-24hours fluctuation is observed. The green colour indicates that the variation s of ROTI on December 21, 2015. In all the seven station the fluctuation is minimum from 0-24hour.

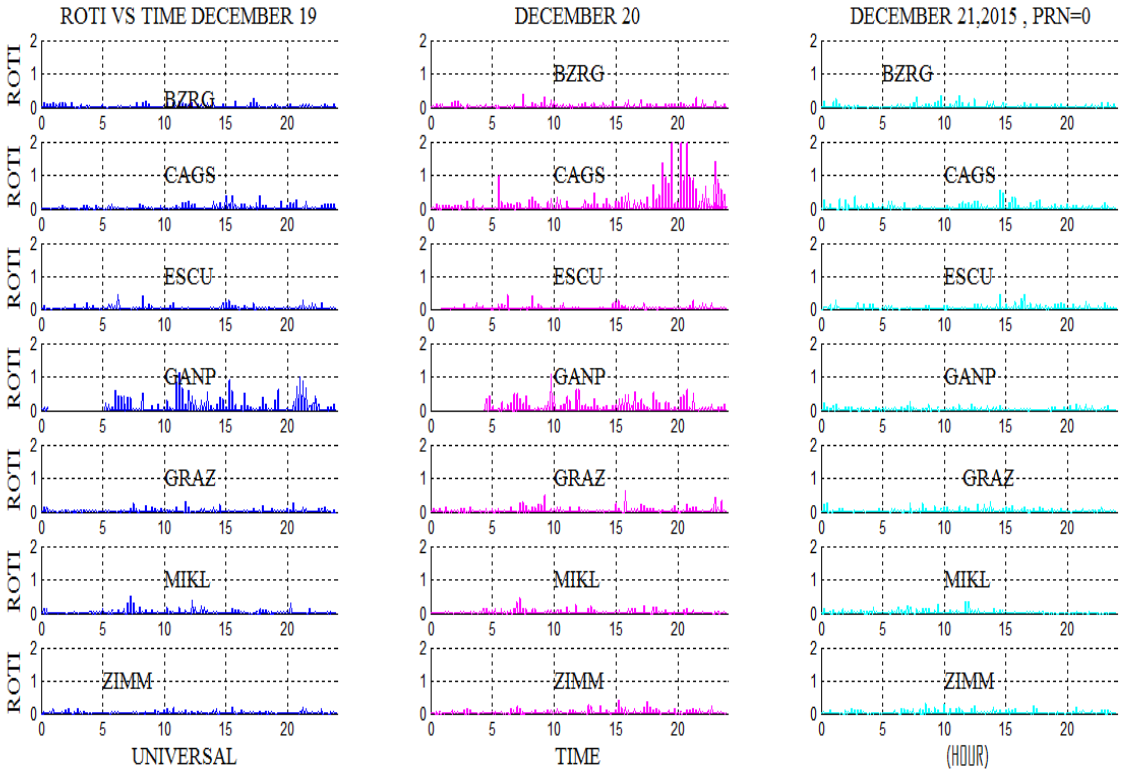

Figure 4. 11*: The variations of ROTI (at PRN = 0) for IGS station (BZRG, CAGS, ESCU, GANP, GRAZ MIKL and ZIMM) site in December (1days:9, 20 &21), 2015.*

In figure 4.11 the vertical axis represents of the ROTI value and the horizontal axis denote time in hours. The PRN numbers of each subfigure is 0. The blue colour shows initial phase, magenta colours as the main phase and the green colour is recovery phase.

The blue colour shows longitudinal variations of Rate of total electron content (ROT) on December 19, 2015.The minimum variations in ROTI is observed over 24 hours at BZRG, CAGS, ESCU, GRAZ, MIKL and ZIMM, 24hour. In the station GANP has variable ROTI between 5-24hours. The magenta colour shows the longitudinal variations of Rate of total electron content index (ROTI) on December 20, 2015. The variations of ROTI at BZRG, ESCU, GRAZ, and MIKL &ZIMM s strong and finally0-24hour more over ROTI exhibits high variability at GANP from 5-24hour. In C AGS 0-19hour is ROTI is low and 19-24hour ROTI is high and the pick value is 2. In GANP 0-5hour have no data and 5-24hors the value of TOTI high. The green colour shows the longitudinal variations of Rate of total electron

content index (ROTI) on December 21, 2015. The variation of ROTI in all IGS stations is observed from 0-24hour. The value of ROTI is observed highly in all the seven IGS station.

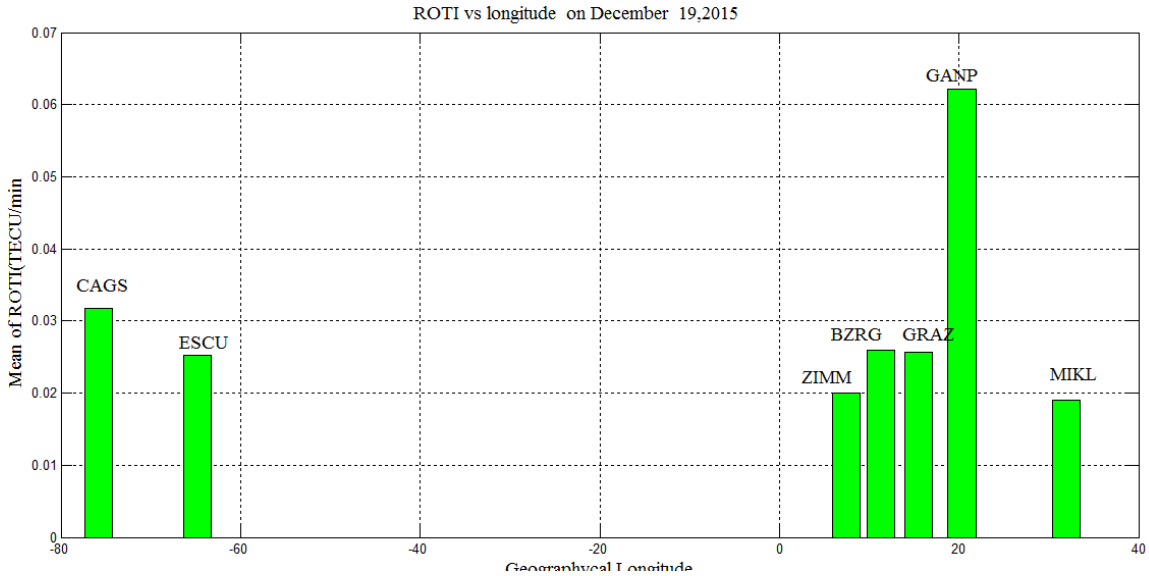

(a)

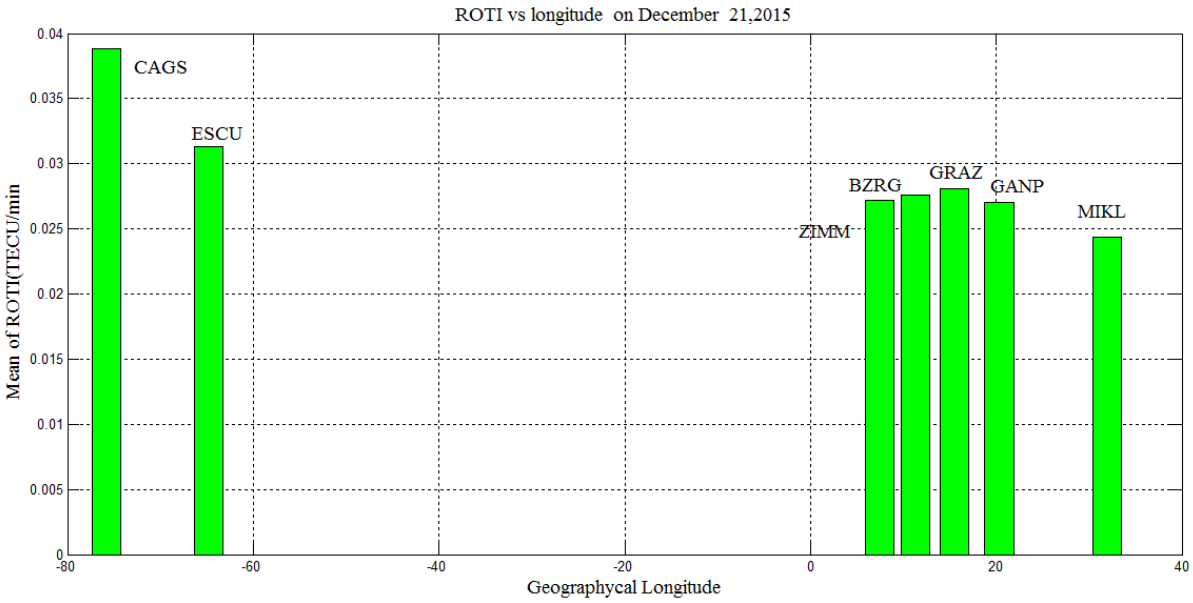

(b)

Figure 4. 12 : The mean of Rate of TEC Index (ROTI) vs Geographical Longitude of the seven stations at PRN=0 in December 19&21, 2015.

In figure 4.12 the horizontal axis represents geographical longitude and the vertical axis represents ROTI. This figure is showed that the longitudinal variations of phase scintillation during geomagnetic storm. Figure (a), (ROTI) is low in 4.12 show low ROTI value Ukraine

(MIKL) and high on Slovakia (GANP) .besides, figure 4.12(b) illustrates low (ROTI) low in Ukraine (MIKL) and high value in Canada (CAGS).

4.3 Conclusion

We obtained that the longitudinal variation of ionospheric phase scintillation characteristics during geomagnetic storm on March 16-19, June 22-24 and December 19-21, 2015. On the 16th of March 2015 strong fluctuation is observed and phase scintillation in Canada (ESCU) in the initial phase. All the rest is observed weak fluctuation. There is no phase scintillation. Since phase scintillation is expressed in rate of change of total electron content index (ROTI). on the 17th of March 2015 is observed strong fluctuation in Canada (ESCU) and in Italy (BZRG) moderate fluctuation and ionospheric phase scintillation is observed Canada, (CAGS), however, station Austral (GANP), Slovakia (GRAZ), Ukraine (MIKL) and Switzerland (ZIMM) observed weak fluctuation the main phase which implies there is no ionospheric scintillation. In March 18, 2015 Italy (BZRG), Canada (CAGS & ESCU) and Austria (GANP) is observed intense or strong fluctuation, in Slavonia -(GRAZ), Ukraine(MIKL) and Swaziland (ZIMM) is observed weak fluctuation, there is no ionospheric phase scintillation. In June(days: 22, 2015 Italy (BZRG)& Austria (GANP) is observed moderate fluctuation, Canada (CAGS & ESCU) , Slavonia(GRAZ),Ukraine(MIKL) and Swaziland (ZIMM) is observed strong fluctuation ,there is phase scintillation .In June 23, 2015 Italy (BZRG), Austria (GANP) ,Slavonia(GRAZ),Ukraine(MIKL) and Swaziland (ZIMM) is observed is observed weak fluctuation which indicates that there is no ionospheric phase scintillation. In contrast the strong variation on ROTI Canada (CAGS and ESCU) is observed strong fluctuation indicates that there is ionospheric phase scintillation. On (days: June 24, 2015 Italy (BZRG), Canada (CAGS & ESCU) and Swaziland (ZIMM) is an observed weak fluctuation which implies that there is no ionospheric phase scintillation, Austria (GANP) and Slavonia(GRAZ) is observed strong fluctuation, Ukraine(MIKL) has moderate fluctuation. On December (days: 19, 2015 moderate fluctuation or phase scintillation is observed in Slovakia (GANP). In December 20, 2015 observed strong fluctuation and phase scintillation in Canada (CAGS). On December (days:21, 2015 weak fluctuation of ROTI observed in all station and as well as there is no fluctuation.

4.4 Recommendation

The work presented in this thesis has shown promising results which in future can be used to understand the longitudinal variations of phase scintillation during geomagnetic storm on GNSS/GPS receivers one can understand that the ionospheric scintillation by using GPS data. This thesis is used to understand the longitudinal variations of phase scintillation during geomagnetic storm over the seven countries which lie along the same latitude (average degree is 47) but different longitude. So, I recommended that in future work, we use VTEC, ROT & ROTI rather than mean of ROTI to study ionospheric phase scintillation during geomagnetic storm.

References

1. Al-Ubaidi and Ali. (2013). Striking Perturbations of Ionospheric Total Electron Content (TEC) During Earthquake. *Iraqi Jornal of science*, Vol.54, No.1, Pp.232-239.
2. Amensisa Negasa, Sreenu Kasam., Baylie D., Melessew N., & A.T.Raghavendra. (2015). Reaction of Ethiopia Ionosphere to Sun based Movement and Geomagnetic Storm. *International Journal of Modern Chemistry and Applied Science*, 2(4), 228-234.
3. Briekke, A. (2013). *Spase of the UpperPolar Atmosphere Second Edition* . London: Acadamic Press.
4. Ephrem Beshir Seba & Melessew Nigussie. (2016). Investigating the effect of geomagnetic storm and equatorial electrojet on equatorial ionospheric irregularity over East African sector. *Advances in Space Research 58 1708–1719*, 58 ,1708–1719.
5. J.S. Xu, J. Z. (2007). Effects of a major storm on GPS amplitude scintillations . *advanced reaserch*, 7,121-167.
6. J.S. Xu, J. Z. (2007). Effects of a major storm on GPS amplitude scintillations . *advanced reaserch*, 7,121-176.
7. J.S. Xu,J. Zhu, L. Li. (2007). Effects of a major storm on GPS amplitude scintillations and. *ADVANCED IN SPCE RESEARCH*, 7.
8. Kai Guo , Yang Liu , Yan Zhao and Jinling Wang. (2016). Analysis of Ionospheric Scintillation Characteristics. *sensors*, 17,111-167.
9. Kallenrode, M.-B. (2004). *space physics An Introdution to Plasma and Particle in the Heiosphere and Magnetospheres ,Third Edition.* Germany: Acadamy Press.
10. Krankowski, S. &. (2012). High latitude TEC fluctuations and irregularity oval during geomagnetic storms. *CrossRef*, Earth Planets Space, 64, 521–529.
11. Michael C.Kelley. (2009). *The Earth's Ionosphere Plasma Physics and Electrodynamics Second Edition.* London: Acadamic Press.
12. Moldwin., M. (2008). *An introduction to space weather*. New York: Cambridge University Press.
13. OLIVAREZ, N. (2013). MITIGATING THE EFFECTS OF IONOSPHERIC SCINTILLATION ON GPS CARRIER RECOVERY. *Research Advance*, 1,1-124.

14. Papagiannis, M. (1972). *Space Physics and Space Astronomy.* New York: Gordon and Breach.

15. Pi, X.,Mannucci, A., Lindqwister and U., Ho, C. (1997). Monitoring of global ionospheric irregularities using the worldwide GPS network. *Geophys. Res. Lett*, 24, 2283–2286.

16. Ratclffe, J. A. (2004). *Physics of the Earths space environment, An introduction.* Verlag Berlin Heidelberg.

17. Rishbeth,H.and Garriott,O.K. (1996). *Introduction to Ionospheric physics.* New York: Acadamic Press.

18. S.Aschwaden, M. (2004). *Physics of the Solar Coronal An Introduction.* London: Advance Press.

19. S.D. Taabu, F.M. D'ujanga and T. Ssenyonga. (2016). Prediction of ionospheric scintillation using neural network over East African region during ascending phase of sunspot cycle 24. *Advances in Space Research xxx) xxx–xxx*, xxx–xxx.

20. Schunck,R. & Nagy,A. (2009). *Ionospheres: Physics,Plasma Physics and Chemistry,Second Edition.* New Work: Combridge University Press.

21. Schunk, R. W. and A. F. Nagy. (2000). *Ionospheres, Physics, Plasma physics and Chemistry.* Cambridge, Atmospheric and Space science series.

22. Y. Sahai F. Becker-Guedes a, P.R. Fagundes a, W.L.C. Lima b and Y. Otsuka c. (2007). Response of nighttime equatorial and low latitude F-region to. *advancein space research*.

23. Y. Sahai,F. Becker-Guedes,P.R. Fagundes,W.L.C. Lima and Y. Otsuka. (2003). Response of nighttime equatorial and low latitude F-region to. *ADVANCE N SPACE RESEARCH*, 10,287-299.

24. Yang, Z. and Liu, Z. (2015). Correlation between ROTI and ionospheric scintillation indices using Hong Kong low-latitude GPS data. *GPS Solut*, 15, 20, 1–10.

25. Yu Jiao and Yu T. Morton. (2015). Comparison of the effect of high-latitude and equatorial ionospheric scintillation on GPS signals during the maximum of solar cycle 24. *RADIO SCIENCE*, 51, 742–753.

DECLARATION

I hereby declare that this thesis is my original work and has not been presented for a degree in any other university, and that all sources of materials have been duly acknowledged.

Name: Agegnehu Sisay Birhan

Signature: _____

Date: _____

This thesis has been submitted for the examination with my approval as a University advisor.

Name: Dr. Tsegaye Kassa

Signature: _____

Date: _____